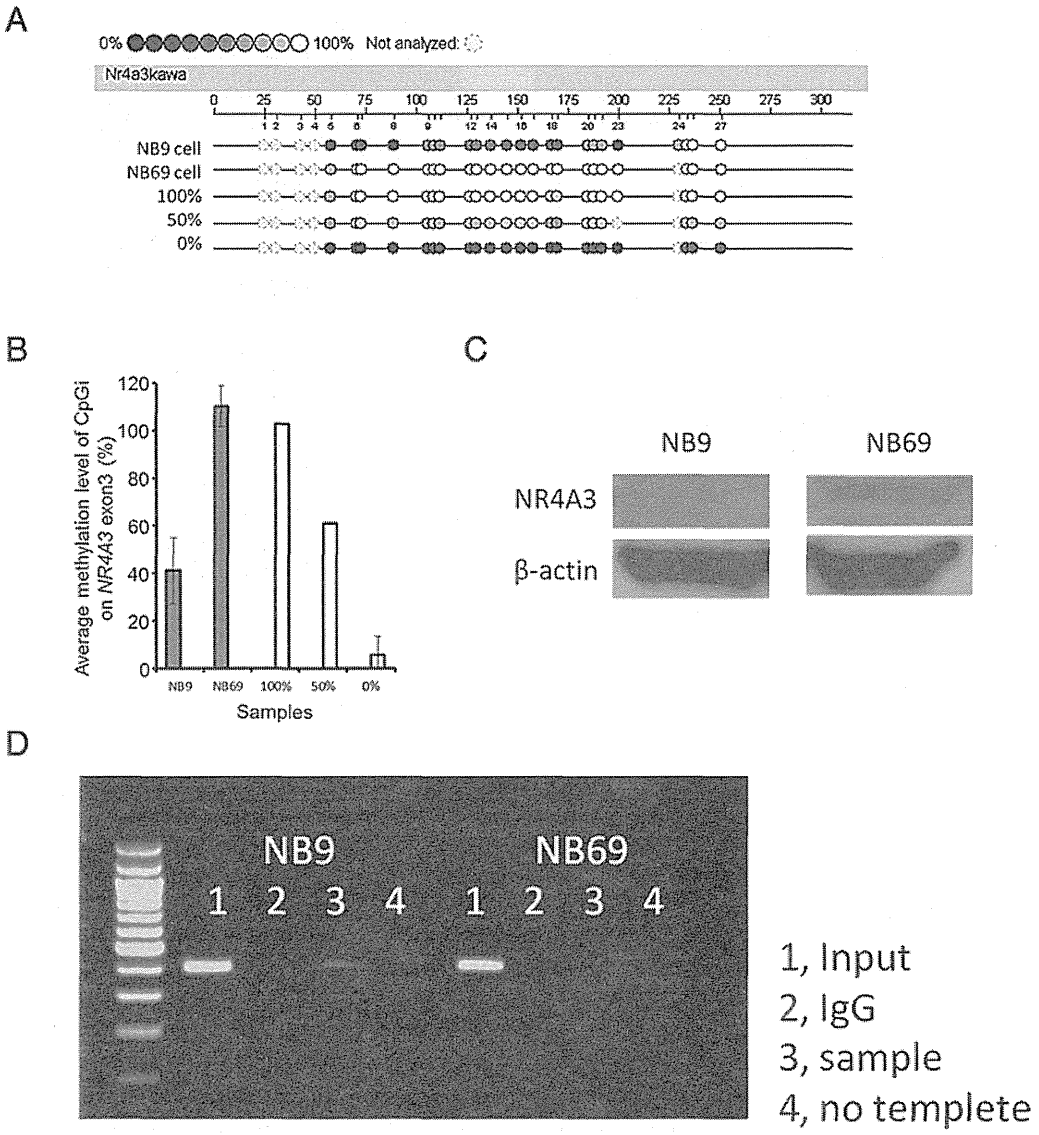

Figure 5. DNA methylation and protein expression levels of NR4A3 in human neuroblastoma cell lines. DNA methylation levels were analyzed quantitatively using Sequenom MassARRAY epiTYPER. (A) Methylation level of each CpG is shown in Epigram. (B) Average methylation level of each CpG site in this region is shown. Gray columns indicate neuroblastoma cell lines and open columns are the standard. Error bars indicate SD. (C) NR4A3 protein expression was analyzed by western blotting. NB69 showed high methylation level of the *NR4A3* gene and expressed NR4A3 protein, while hypomethylated NB9 cells did not express the protein. (D) Chromatin immunoprecipitation assay of NR4A3 exon 3 region. Crosslinked DNA-protein complexes were immunoprecipitated with anti-CTCF antibody and control antibodies, followed by PCR amplification using primers for NR4A3 exon 3. Precipitant from NB9 lysate contained NR4A3 exon 3 region, but no product was amplified in the precipitant from NB69 lysate.

7% 5'-untranslated region (UTR), 3% exonic, 29% intronic and 20% within 2.5 kb of promoters. H19 DMR is one of CTCF-binding sites and its methylation level is related to epigenetic remodeling, which is co-localized with cohesion. Aberrant regulation of CTCF expression is associated with occurrence of cancers, such as colorectal carcinoma (18,30,31). Our present study showed that CTCF can coimmunoprecipitate with a CTCF binding site within *NR4A3* exon 3 CpGi in NB9 cells but not in NB69 cells. This suggests hypermethylation of *NR4A3* exon 3 CpGi in NB69 cells may inhibit its binding to the CTCF and therefore initiate expression of NOR1. This expression regulation via CTCF binding may be a mechanism of NOR1 down-regulation and involved in advanced neuroblastomas and/or neuronal de-differentiation.

This is the first report indicating that DNA methylation level of *NR4A3* exon 3 CpGi is associated with NOR1 expression and aberrantly methylated in neuroblastomas. In addition, our present data suggest that hypermethylation of this region might be one of the prognostic factors in this tumor. Although further analyses are necessary to elucidate the regulation mechanism of NOR1 expression and its function, our present data strongly suggest that this gene could be involved in neural differentiation and human neuroblastomagenesis.

Acknowledgements

This study was supported by Nihon University Multidisciplinary Research Grant for 2006 (to H.N.), the Academic Frontier

Project for 2006 Project for Private Universities, a matching fund subsidy from MEXT (to H.N.), National Cancer Institute Grant CA102423 (to W.A.H and H.N.), National Cancer Institute Center Support Grant CA16056 (to Roswell Park Cancer Institute) and Grant-in-Aid from the Ministry of Education, Science, Sports and Culture of Japan (grant nos. 20592092 and 23300344).

References

1. De Bernardi B, Nicolas B, Boni L, Indolfi P, Carli M, Cordero Di Montezemolo L, Donfrancesco A, Pession A, Provenzi M, di Cataldo A, Rizzo A, Tonini GP, Dallorso S, Conte M, Gambini C, Garaventa A, Bonetti F, Zanazzo A, D'Angelo P and Bruzzi P: Disseminated neuroblastoma in children older than one year at diagnosis: comparable results with three consecutive high-dose protocols adapted by the Italian Co-Operative Group for Neurobalstoma. J Clin Oncol 21: 1592-1601, 2003.
2. Matthay KK, Villablanca JG, Seeger RC, Stram DO, Harris RE, Ramsay NK, Swift P, Shimada H, Black CT, Brodeur GM, Gerbing RB and Reynolds CP: Treatment of high-risk neuroblsatoma with intensive chemotherapy, radiotherapy, autologous bone marrow transplantation, and 13-cis-retinoic acid. Children's Cancer Group. N Engl J Med 341: 1165-1173, 1999.
3. Wang H, Lee S, Nigro CL, Lattanzio L, Merlano M, Monteverde M, Matin R, Purdie K, Mladkova N, Bergamaschi D, Harwood C, Syed N, Szlosarek P, Briasoulis E, McHugh A, Thompson A, Evans A, Leigh I, Fleming C, Inman GJ, Hatzimichael E, Proby C and Crook T: NT5E (CD73) is epigenetically regulated in malignant melanoma and associated with metastatic site specificity. Br J Cancer 106: 1446-1452, 2012.
4. Geiman TM and Muegge K: DNA methylation in early development. Mol Reprod Dev 77: 105-113, 2010.
5. Bird A: DNA methylation patterns and epigenetic memory. Genes Dev 16: 6-21, 2002.
6. Weber M, Hellmann I, Stadler MB, Ramos L, Pääbo S, Rebhan M and Schübeler D: Distribution, silencing potential and evolutionary impact of promoter DNA methylation in the human genome. Nat Genet 39: 457-466, 2007.
7. Song F, Smith JF, Kimura MT, Morrow AD, Matsuyama T, Nagase H and Held WA: Association of tissue-specific differentially methylated regions (TDMs) with differential gene expression. Proc Natl Acad Sci USA 102: 3336-3341, 2005.
8. Eckhardt F, Lewin J, Cortese R, Rakyan VK, Attwood J, Burger M, Burton J, Cox TV, Davies R, Down TA, Haefliger C, Horton R, Howe K, Jackson DK, Kunde J, Koenig C, Liddle J, Niblett D, Otto T, Pettett R, Seemann S, Thompson C, West T, Rogers J, Olek A, Berlin K and Beck S: DNA methylation profiling of human chromosomes 6, 20 and 22. Nat Genet 38: 1378-1385, 2006.
9. Zhao Y and Bruemmer D: NR4A orphan nuclear receptors: transcriptional regulators of gene expression in metabolism and vascular biology. Arterioscler Thromb Vasc Biol 30: 1535-1541, 2010.
10. Maxwell MA and Muscat GE: The NR4A subgroup: immediate early response genes with pleiotropic physiological roles. Nucl Recept Signal 4: e002, 2006.
11. Song F, Mahmood S, Ghosh S, Liang P, Smiraglia DJ, Nagase H and Held WA: Tissue specific differentially methylated regions (TDMR): Changes in DNA methylation during development. Genomics 93: 130-139, 2009.
12. Li LC and Dahiya R: MethPrimer: designing primers for methylation PCRs. Bioinformatics 18: 1427-1431, 2002.
13. Ehrich M, Nelson MR, Stanssens P, Zabeau M, Liloglou T, Xinarianos G, Cantor CR, Field JK and van den Boom D: Quantitative high-throughput analysis of DNA methylation patterns by base-specific cleavage and mass spectrometry. Proc Natl Acad Sci USA 102: 15785-15790, 2005.
14. Fatemi M, Pao MM, Jeong S, Gal-Yam EN, Egger G, Weisenberger DJ and Jones PA: Footprinting of mammalian promoters: use of a CpG DNA mehtyltransferase revealing nucreosome positions at a single molecule level. Nucleic Acids Res 33: e176, 2005.
15. Baxter EW, Cummings WJ and Fournier REK: Formation of a large, complex domain of histone hyperacetylation at human 14q32.1 requires the serpin locus control region. Nucleic Acids Res 33: 3313-3322, 2005.
16. Orlando V, Strutt H and Paro R: Analysis of chromatin structure by in vivo formaldehyde cross-linking. Methods 11: 205-214, 1997.
17. Bowers SR, Mirabella F, Calero-Nieto FJ, Valeaux S, Hadjur S, Baxter EW, Merkenschlager M and Cockerill PN: A conserved insulator that recruits CTCF and cohesin exists between the closely related but divergently regulated interleukin-3 and granulocyte-macrophage colony-stimulating factor genes. Mol Cell Biol 29: 1682-1693, 2009.
18. Ishihara K, Oshimura M and Nakao M: CTCF-dependent chromatin insulator is linked to epigenetic remodeling. Mol Cell 23: 733-742, 2006.
19. Akoben AK: Understanding diagnostic tests 3: Receiver operating characteristic curves. Acta Paediatr 96: 644-647, 2007.
20. Egger G, Liang G, Aparicio A and Jones PA: Epigenetics in human disease and prospects for epigenetic therapy. Nature 27: 457-463, 2004.
21. Laird PW: Cancer epigenetics. Hum Mol Genet 15: 65-76, 2005.
22. Gonzalez-Gomez P, Bello MJ, Lomas J, Arjona D, Alonso ME, Amiñoso C, Lopez-Marin I, Anselmo NP, Sarasa JL, Gutierrez M, Casartelli C and Rey JA: Aberrant methylation of multiple genes in neuroblastic tumours. relationship with MYCN amplification and allelic status at 1p. Eur J Cancer 39: 1478-1485, 2003.
23. Banelli B, Vinci AD, Gelvi I, Casciano I, Allemanni G, Bonassi S and Romani M: DNA methylation in neuroblastic tumors. Cancer Lett 228: 37-41, 2005.
24. Kawashima H, Sugito K, Yoshizawa S, Uekusa S, Furuya T, Ikeda T, Koshinaga T, Shinojima Y, Hasegawa R, Mishra R, Igarashi J, Kimura M, Wang X, Fujiwara K, Gosh S and Nagase H: DNA hypomethylation at the ZNF206-exon 5 CpG island associated with neuronal differentiation in mice and development of neuroblastoma in humans. Int J Oncol 40: 31-39, 2012.
25. Zetterström RH, Williams R, Perlmann T and Olson L: Cellular expression of the immediate early transcription factors Nurr1 and NGFI-B suggests a gene regulatory role in several brain regions including the nigrostriatal dopamine system. Brain Res Mol Brain Res 5: 111-120, 1996.
26. Ohkura N, Ito M, Tsukada T, Sasaki K, Yamaguchi K and Miki K: Structure, mapping and expression of a human NOR-1 gene, the third member of the Nur77/NGFI-B family. Biochim Biophys Acta 1308: 205-214, 1996.
27. Eells JB, Wilcots J, Sisk S and Guo-Ross SX: NR4A gene expression is dynamically regulated in the ventral tegmental area dopamine neurons and is related to expression of dopamine neurotransmission genes. J Mol Neurosci 46: 545-553, 2012.
28. Werme M, Ringholm A, Olson L and Brené S: Differential patterns of induction of NGFI-B, Nor1 and c-fos mRNAs in striatal subregions by haloperidol and clozapine. Brain Res 863: 112-119, 2000.
29. Boldingh Debernard KA, Mathisen GH and Paulsen RE: Differences in NGFI-B, Nurr1, and NOR-1 expression and nucleocytoplasmic translocation in glutamate-treated neurons. Neurochem Int 61: 79-88, 2012.
30. Wendt KS, Yoshida K, Itoh T, Bando M, Koch B, Schirghuber E, Tsutsumi S, Nagae G, Ishihara K, Mishiro T, Yahata K, Imamoto F, Aburatani H, Nakao M, Imamoto N, Maeshima K, Shirahige K and Peters JM: Cohesin mediates transcriptional insulation by CCCTC-binding factor. Nature 451: 796-801, 2008.
31. Phillips JE and Corces VG: CTCF: master weaver of the genome. Cell 137: 1194-1211, 2009.

Pediatr Blood Cancer 2014;61:1184–1189

Bilateral Wilms Tumors Treated According to the Japan Wilms Tumor Study Group Protocol

Takaharu Oue, MD, PhD,[1]* Tsugumichi Koshinaga, MD, PhD,[2] Hajime Okita, MD, PhD,[3] Yasuhiko Kaneko, MD, PhD,[4] Shiro Hinotsu, MD, PhD,[5] and Masahiro Fukuzawa, MD, PhD[6]

Background. The introduction of multimodal therapy has improved the survival rate of bilateral Wilms tumors (BWT); however, the results are still not satisfactory in terms of the renal preservation. To establish a new treatment strategy for BWT, we reviewed the results of the cases registered in the Japan Wilms Tumor Study Group (JWiTS). ***Procedure.*** This analysis concerned patients with synchronous BWT registered in the JWiTS between 1996 and 2011. In these patients, the management of BWT included initial tumor resection or biopsy followed by chemotherapy. The details of the treatments and outcomes were analyzed. ***Results.*** Among the 355 cases registered in the JWiTS database, 31 (8.7%) had BWT. They were 16 males and 15 females with a mean age of 15.5 months. Preoperative chemotherapy was performed in 24 cases. Bilateral nephron-sparing surgery (NSS) was achieved in 10 of 28 cases (36%). All of the cases were of favorable nephroblastoma without anaplasia, and a *WT1* mutation was detected in 21 of the 27 cases (78%) examined. The 5-year overall survival was 92.6%; however, 10 children (40%) developed impaired renal function and three of them developed renal failure. ***Conclusions.*** The long-term survival rates for patients with synchronous BWT have improved. However, more than half of patients receive nephrectomy. The protocol should be changed to improve the rate of preservation of the renal parenchyma. Preoperative chemotherapy should be performed to shrink the tumors in every case, and subsequent NSS should be carried out after a central imaging evaluation. Pediatr Blood Cancer 2014;61:1184–1189.

Key words: bilateral; chemotherapy; JWiTS; nephron-sparing surgery; Wilms tumor

INTRODUCTION

About 5% of patients with Wilms tumors (nephroblastomas) have synchronous bilateral tumors [1–5]. In these cases, both local tumor control and preservation of the renal function are necessary. However, the optimal management for these patients remains to be defined.

The Japan Wilms Tumor Study (JWiTS) group was founded in 1996, and a nationwide multicenter cooperative study (JWiTS-1) was started to improve the outcomes of children with renal tumors [6]. In this study, the management of bilateral Wilms tumor (BWT) included initial biopsy or tumor resection, followed by chemotherapy, according to the abdominal stage and histological features. The surgeons were recommended to preserve renal function without compromising cancer control.

The preliminary results of JWiTS-1 study conducted between 1996 and 2005 have shown that the prognosis of bilateral nephroblastoma was fair; the 5-year OS rate for patients with BWT was 78.7% [6]. However, nephrectomy and partial resection of the opposite kidney was performed in seven cases, and bilateral nephrectomy was performed in one case. Finally, two patients experienced renal failure and required dialysis or renal transplantation. These results were not satisfactory, and the protocol for the treatment of BWT should be changed to emphasize renal preservation.

Before starting a new protocol study, we retrospectively reviewed the management and outcome of patients with BWT previously registered in the Japan Wilms Tumor Study Group (JWiTS) in order to clarify the outcomes and problems of the present protocol. These results will be informative and help to create the new protocol, and can be the historical control for the new protocol study.

MATERIALS AND METHODS

Patients and Treatments

Between 1996 and 2011, 355 cases with pediatric renal tumors were registered in the JWiTS database. Among them, 31 (8.7%) were synchronous BWTs (Stage 5). These patients were 16 males and 15 females. The clinical and epidemiological data at diagnosis were extracted from registry files. Information about the chemotherapy regimen used, as well as the surgical, histological and imaging records, were collected and reviewed. Most of these patients were treated according to the JWiTS-1 protocol (1996–2005) and JWiTS-2 protocol (2005–2011), which was similar to the NWTS-5 protocol, but the protocol was sometimes modified by the local institutions. In this protocol, the management of BWT consisted of initial biopsy or tumor resection, followed by chemotherapy, according to the abdominal stage and histological features. The surgeons were recommended to perform nephron-sparing surgery (NSS; partial nephrectomy, wedge resection or tumor enucleation) in order to preserve the renal function as much as possible.

The response to treatment was evaluated as follows: *Complete Response* (*CR*): disappearance of the tumor; *Partial Response* (*PR*): at least a 30% decrease in the longest diameter (LD) of the tumor; *Stable Disease* (*SD*): neither sufficient shrinkage to qualify for PR nor a sufficient increase to qualify for PD; *Progressive Disease* (*PD*): at least a 20% increase in the LD of the tumor or the appearance of one or more new tumors. In patients whose frozen tumor tissue was available, a *WT1* mutation analysis was performed

[1]Department of Pediatric Surgery, Osaka University Graduate School of Medicine, Osaka, Japan; [2]Department of Pediatric Surgery, Nihon University School of Medicine, Tokyo, Japan; [3]National Center for Child Health and Development, Tokyo, Japan; [4]Research Institute for Clinical Oncology, Saitama Cancer Center, Saitama, Japan; [5]Center for Innovative Clinical Medicine, Okayama University Hospital, Okayama, Japan; [6]Osaka Medical Center and Research Institute for Maternal and Child Health, Osaka, Japan

Conflict of interest: Nothing to declare.

*Correspondence to: Takaharu Oue, Department of Pediatric Surgery, Osaka University Graduate School of Medicine, 2-2 Yamadaoka, Suita, Osaka 565-0871, Japan. E-mail:ooue@pedsurg.med.osaka-u.ac.jp

Received 13 September 2013; Accepted 17 January 2014

DOI 10.1002/pbc.24979
Published online 12 February 2014 in Wiley Online Library (wileyonlinelibrary.com).

using PCR direct sequencing of all 10 exons, as previously described [7].

Statistical Analysis

The overall survival (OS) was defined as the time from the date of registration to death from any cause or to the date of the last follow-up, and the event-free survival (EFS) was defined as the time from the date of registration to death from any cause or to the first occurrence of tumor recurrence (local or metastasis) or progression. The OS and EFS were calculated using the Kaplan–Meier method [8]. All *P*-values were two-sided, and values <0.05 were considered to be statistically significant. All statistical analyses were performed using the JMP version 9.02 (SAS Institute Japan, Tokyo, Japan).

RESULTS

Patient Characteristics

The mean age of the patients at presentation was 15.5 ± 13.0 months (range: 7–62 months), which was younger than the age of the 324 children with unilateral tumors (26.0 months) ($P < 0.001$). Six patients (19%) had associated genitourinary abnormalities (undescended testis: n = 4, hypospadias: n = 3, horseshoe kidney: n = 1). Two patients were diagnosed with Denys–Drash Syndrome (DDS), both of whom had a *WT1* mutation in the tumor tissue: a male patient with hypospadias and an undescended testis, and a female patient with no genitourinary abnormalities. No patients exhibited Beckwith–Wiedemann syndrome, WAGR syndrome, isolated hemihypertrophy, cryptorchidism or a double collecting system in our series. One patient had a family history of Wilms tumor. One patient (3.2%) had lung metastases at diagnosis, and another one (3.2%) had abdominal lymph node metastasis (Table I).

TABLE I. Characteristics of the 31 Cases With Bilateral Wilms Tumors

Characteristics	N	%
Age Average 15.5 ± 13.0 months (range: 7–62 months)		
Sex		
Male	16	52
Female	15	48
Associated anomalies		
Yes	6[a]	19
No	25	81
Associated syndrome		
Yes	2[b]	6
No	29	94
Histology		
Favorable nephroblastoma	31	100
Anaplasia	0	0
Metastasis at diagnosis		
Yes	2	6
No	29	94

[a]Undescended testis: 4 (13%), hypospadias: 3 (10%), horseshoe kidney: 1 (3%); [b]Denys–Drash syndrome: 2 (6%).

Initial Biopsy, Preoperative Chemotherapy, and Radiation Therapy

The details of the treatment were obtained from the pediatricians for 28 cases (90%). Preoperative chemotherapy was performed in 24 cases. Among them, a tumor biopsy was performed before chemotherapy in 17 cases (71%). The remaining four cases underwent primary tumor resection. The mean duration of preoperative chemotherapy was 14.2 weeks (8–24 weeks). The initial treatment regimens were EE-4A (vincristine and dactinomycin) in 11 cases and DD-4A (vincristine, dactinomycin, and doxorubicin) in 13 cases. The selection of EE-4A or DD-4A as the initial chemotherapy regimen was based on the higher local (abdominal) stage of each kidney according to the NWTS-V protocol; however, these guidelines are sometimes modified by local institutions. In nine cases, a modification of the chemotherapy regimen was decided in order to improve the tumor response (upgrade from EE-4A to DD-4A, or use of other drugs, such as cyclophosphamide and carboplatin). The imaging studies revealed that the response to the initial chemotherapy was evaluated as PR for both sides in eight patients, PR and NC for each side in two patients, NC for both sides in 11 patients and PR and PD for each side in three patients. Therefore, a significant tumor response was observed in 21 of the 48 kidneys. One patient with lung metastasis achieved a CR of the metastatic region during the preoperative chemotherapy. Four patients received radiation therapy, three for tumors before resection and one for the tumor bed after resection. The median dose of radiation was 16 Gy (range: 10–30 Gy). One patient with lung metastases did not receive radiation treatment for the lung.

Surgery

The details of the surgery were obtained for 28 cases. Twelve children (43%) underwent surgery on both kidneys at the time of the initial procedure. The remaining patients received surgery using a staged approach. For five patients, staged surgery was performed within 8 weeks, and none of these patients received chemotherapy between surgeries. For the remaining 11 patients, the time interval between the two surgeries was longer, and these patients received chemotherapy between the two surgical steps. Ten (36%) children underwent bilateral NSS. All of them received preoperative chemotherapy. Fifteen (54%) underwent total nephrectomy for one kidney and NSS for the contralateral kidney. Three underwent bilateral nephrectomy. Finally, 35 of the 56 kidneys (56%) had been subjected to NSS.

The approximate percentage of residual renal parenchyma in each kidney was estimated by the surgeon and reported in the operative records. Data for both the tumor size and approximate percentage of the residual renal parenchyma were obtained in 24 patients (48 kidneys). There was a significant negative correlation between the tumor size (longer axis measured in the horizontal CT imaging results) and approximate percentage of the residual renal parenchyma indicated in the surgical records (Correlation coefficient $r = -0.48$, $P < 0.01$, Fig. 1). Based on these results, it seems to be difficult to perform NSS when the tumor size exceeds 10 cm.

Pathology and Biology

A central pathological diagnosis was obtained in 30 cases. All of the tumors were diagnosed as favorable nephroblastomas without

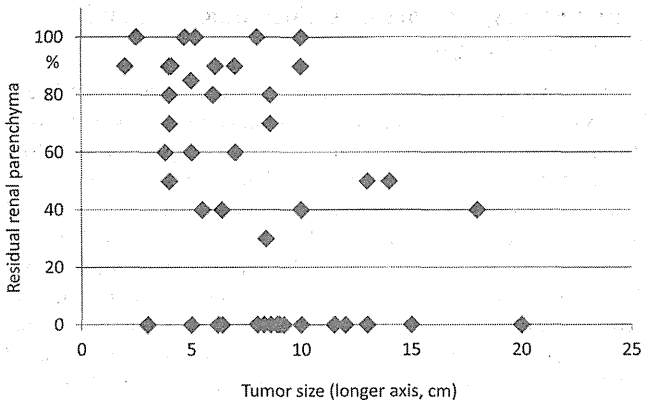

Fig. 1. The relationship between the tumor size and the percentage of the residual renal parenchyma. Data for both the tumor size and approximate percentage of the residual renal parenchyma were obtained in 24 patients (48 kidneys). Some markers were very close to or overlapped with each other, such that the number of markers appears to be less than 48. There was a negative correlation between the tumor size (longer axis measured in the horizontal CT images) and the approximate percentage of the residual renal parenchyma indicated in the surgical records (Correlation coefficient $r = -0.48$, $P < 0.01$).

anaplasia. In 11 tumors (37%), the skeletal muscle component dominated, and the tumors were diagnosed as fetal rhabdomyomatous nephroblastoma (FRN). The *WT1* gene was analyzed in the tumor tissues in 27 cases, and a mutation was detected in 21 of these cases (78%). All six cases associated with a genitourinary abnormality had a *WT1* mutation in their tumors.

Outcome

Follow-up data were available for 30 cases, and two patients died during the follow-up period; one of disease and one of infection. The median follow-up duration was 8.0 years (range: 1.3–13.1 years). The 5-year EFS and OS rates were 85.5% and 92.6%, respectively, (Fig. 2). The 5-year OS and EFS rates of the 10 children who underwent bilateral NSS were both 100%, whereas the 5-year OS and EFS rates of the 20 children who underwent complete nephrectomy or the removal of at least one kidney were 93.8% and 81.3%, respectively. However, there were no statistical differences between the two groups (log-rank test, $P = 0.51$ for OS and $P = 0.21$ for EFS). Three patients (13%) relapsed; there was one local relapse and two metastatic relapses to the lungs. Two patients entered a second CR after resection of the lung metastasis and chemotherapy; however, one patient died of local relapse.

Renal Function

The renal function was followed in 25 cases. The renal function was assessed at the local hospital in the clinic according to the levels of serum creatinine, BUN, electrolytes and urinary parameters. A serum creatinine and/or BUN level elevated 1.5 times the maximum of the normal range indicated an impaired renal function, as observed in 10 children (40%). Among these patients, four eventually developed renal failure requiring hemodialysis (HD). Renal transplant was carried out in one of these patients. The 5- and 10-year survival rates with the native kidney (survival without HD or renal transplantation) among the patients without DDS were 85.1% and 78.3%, respectively, while those among the patients with a normal renal function were 85.1% and 52.8%, respectively (Fig. 3). Figure 4 shows the survival rates for the patients with a native kidney and those with a normal renal function among the subjects who did (Bil NSS (±)) and did not (Bil NSS (−)) undergo bilateral NSS. The survival rates of both groups were higher among the patients who underwent bilateral NSS; however, the differences were not statistically significant.

Figure 5 shows the relationship between the percentage of residual renal parenchyma (left % + right %) and the renal function during the long-term follow-up. The patients with residual renal parenchyma estimated to be greater than that of a single kidney (100%) had a normal renal function. On the other hand, most of the patients with residual renal parenchyma estimated to be less than that of a single kidney developed an impaired renal function after

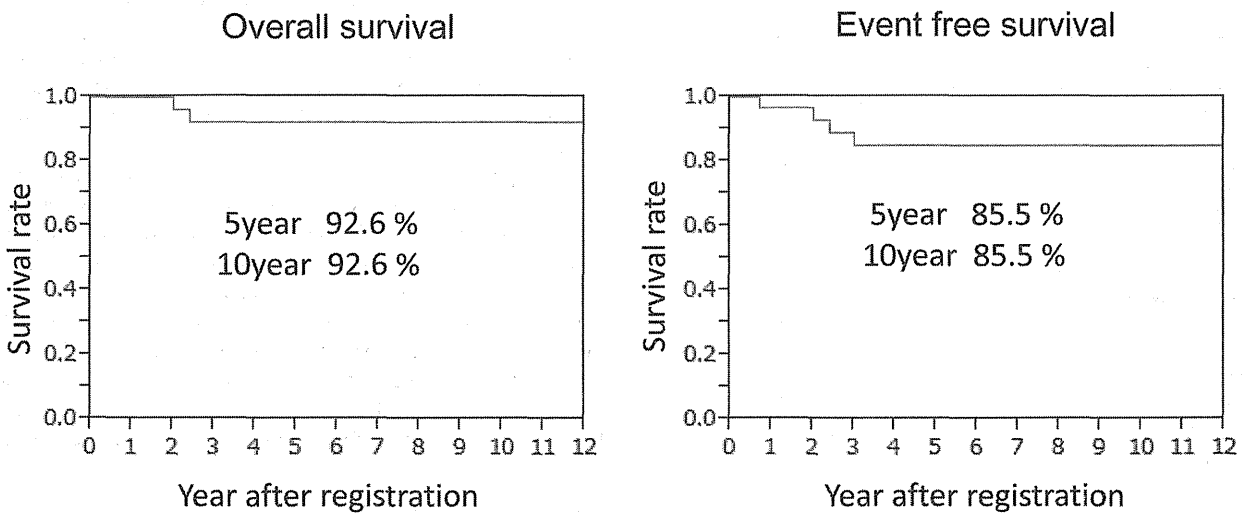

Fig. 2. The overall survival (left, OS) and event-free survival (right, EFS) of the patients with bilateral Wilms tumor registered in the Japan Wilms Tumor Study Group.

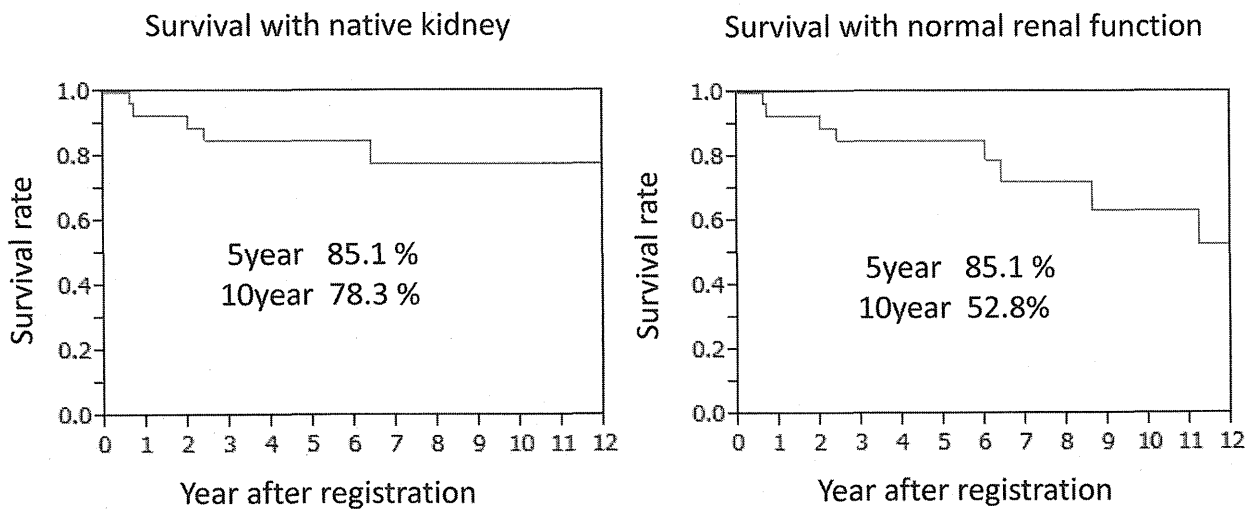

Fig. 3. The survival with a native kidney (right; survival without hemodialysis or a renal transplant) and survival with normal renal function (left). Two patients with Denys–Drash syndrome were excluded.

10 years of follow-up. Two patients who received radiation treatment and another two with Denys–Drash syndrome developed impaired renal function earlier, within 8 years.

DISCUSSION

The results in our population were in agreement with those of previous studies on bilateral WT. There was a similar incidence (3–8%) of bilateral involvement, mean age of the affected patients (15.5 months), and similar incidence of congenital abnormalities [1–5,9–14]. The outcomes for patients with bilateral WT in our study were favorable; the 5-year OS and EFS rates were 92.6% and 85.5%, respectively. These results are similar to the report about the SIOP 93 protocol [15] (89.5% and 83.4% at 5 years) and slightly better than the figures reported by Shamberger et al. [3] (OS of 82.1% at 10 years). These results suggest that the long-term

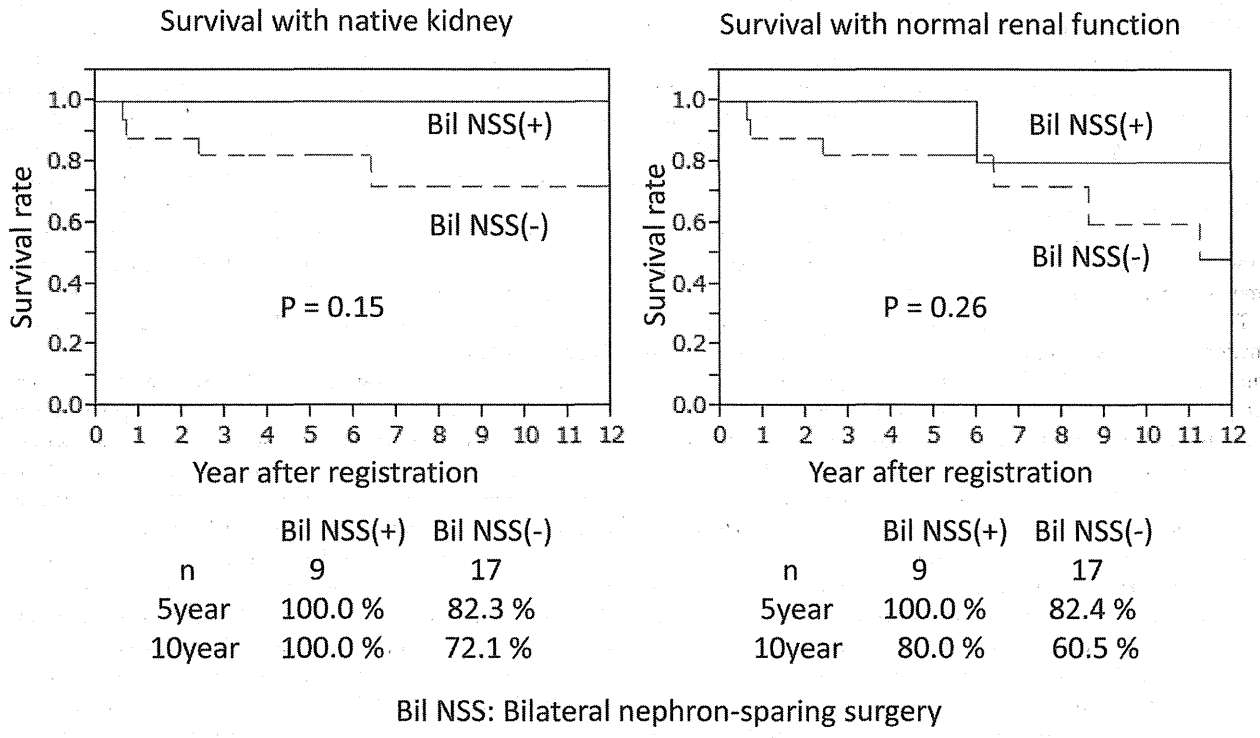

	Bil NSS(+)	Bil NSS(-)
n	9	17
5year	100.0 %	82.3 %
10year	100.0 %	72.1 %

	Bil NSS(+)	Bil NSS(-)
n	9	17
5year	100.0 %	82.4 %
10year	80.0 %	60.5 %

Bil NSS: Bilateral nephron-sparing surgery

Fig. 4. The survival rates of the patients with a native kidney and those with a normal renal function among the patients who did (Bil NSS (+)) and did not (Bil NSS (−)) undergo bilateral NSS. The survival rates of both groups were higher among the patients who underwent bilateral NSS; however, the differences were not statistically significant.

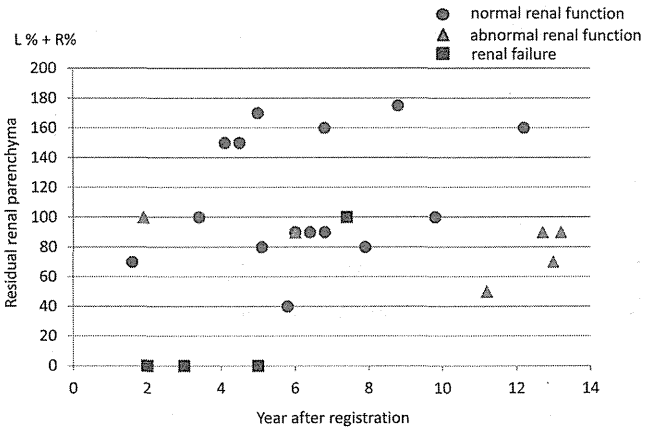

Fig. 5. The relationship between the percentage of the residual renal parenchyma (left % + right %) and renal function during the long-term follow-up in 25 patients. Two markers (circle and triangle) are almost overlapping at 6 years (90%).

survival rates for patients with synchronous bilateral WTs are satisfactory.

However concerning the renal preservation, the percentage of NSS was only 56% of the 56 kidneys. These results were lower than those of the SIOP 93 series; Sudour et al. [15] reported that 3 months of preoperative chemotherapy allowed them to perform NSS in 67% of the kidneys. Therefore, we consider that preoperative chemotherapy should be performed in every patient in the next JWiTS protocol. Perhaps the highest rate of nephron-sparing surgery in bilateral WT was reported by Davidoff et al. [16]. In this single-institution series, 10/12 patients had bilateral NSS. The results for a small number of patients treated at a single center cannot necessarily be translated to a multi-site study; however, these findings indicate that it is worthwhile to aim for a high level of NSS.

In our series, there was a negative correlation between the tumor size and percentage of residual renal parenchyma. The possibility of performing NSS may be decreased when the tumor size exceeds 10 cm at the time of diagnosis. On the other hand, in some cases, NSS was impossible even when the tumor size was less than 5 cm. In these cases, the ability to perform NSS depends not only on the tumor size, but also on the tumor location.

The optimal timing for NSS in order to preserve the renal function without jeopardizing the patient outcome was decided mainly by surgeons. The mean duration of preoperative chemotherapy was 14.2 weeks in our series, which was almost the same as the mean treatment duration of 80 days in the SIOP98 study and median treatment duration of 159 days in the NWTS-4 study [15,17]. These results indicate that most of the children were operated on around 3 months after the diagnosis. Therefore, 3 months seems to be an appropriate duration of preoperative chemotherapy. However, the optimal timing of the NSS is different for each patient, and depends on the response to preoperative chemotherapy. To determine the objective timing of NSS, we are planning to introduce the use of a central imaging evaluation system in the next JWiTS protocol.

In our series, the pathological review revealed that all of the cases were favorable type nephroblastomas, and there were no anaplastic cases. These results suggest that most of the Japanese BWTs are favorable nephroblastomas. Therefore, we consider that a tumor biopsy is not necessary prior to chemotherapy.

During the long-term follow-up, the most significant morbidity was renal dysfunction. Ten of 25 children (40%) developed impaired renal function (elevation of the serum creatine or BUN level) and three of them developed renal failure (requiring hemodialysis or a renal transplant). The 5- and 10-year survival rates with normal renal function were 85.1% and 52.8%, respectively. Lange et al. [18] assessed risk factors for end-stage renal disease among patients with WT without *WT1*-related syndromes and reported that the incidence of end-stage renal disease was 4.0% at 3 years after diagnosis in patients with synchronous bilateral Wilms tumors and 19.3% in those with metachronous bilateral Wilms tumors. The incidence of end-stage renal disease in our series was slightly higher than these previously reported rates: the 5-year survival rate without HD or renal transplantation was 85.1%. One reason for this difference is that our series included more patients who did not undergo bilateral NSS. In the present study, the survival rates of both the patients with a native kidney and those with a normal renal function were lower among the subjects who did not undergo bilateral NSS.

The risk of renal dysfunction was increased in patients with a loss of more than half the renal mass. Most of the patients with residual renal parenchyma estimated to be less than that of a single kidney developed an impaired renal function after 10 years of follow-up. These results indicate that the renal function will slowly be impaired even after 10 years, especially in the patients whose residual renal parenchyma is less than the equivalent of one kidney.

In the present study, the incidence of the *WT1* mutation was higher than that observed in previous series. In 2001, we reported that the *WT1* mutation was found in tumor tissue obtained from only one of five patients with bilateral Wilms tumors [19], whereas in the present series, mutations were detected in 21 of 27 cases (78%). One reasons for this discrepancy is that detection methods have markedly improved over the past 10 years. Currently, researchers use the SNP array method, the sensitivity of which is much higher than that of previous methods [20]. In 2001, only one mutation was detected among five bilateral Wilms tumors; however, the SNP array method enabled us to detect three more mutations in these five cases. Another reason for the above discrepancy is that the incidence of the *WT1* mutation may be higher in Japanese patients than in Western populations [21]. We therefore consider that the genetic background of BWT differs between Japanese and Caucasians [19,21].

According to Breslow et al. [22,23], the development of nephropathy may be associated with *WT1* gene mutations responsible for an alteration of the protein. In this series, the *WT1* mutation was analyzed in the tumor tissues only. However, most patients with the *WT1* mutation in the tumor tissue are considered to also have the somatic *WT1* mutation. Our results indicate that the majority of Japanese children with BWT have a *WT1* mutation, and we consider that some Japanese patients with BWT have a germline mutation of the *WT1* gene. In order to confirm this hypothesis, we plan to analyze the incidence of germline mutations of the *WT1* gene in the next JWiTS protocol study for BWT. Children with WAGR or Denys–Drash syndromes, or those suffering from aniridia or isolated genitourinary abnormalities are at a higher risk of renal failure, independent of the type of treatment [24,25].

Patients with germline mutations of the *WT1* gene may have a high risk of developing nephropathy, which impairs the renal function over the long-term. Grigoriev et al. [26] examined the outcomes of 173 children enrolled in the National Wilms Tumor Study who developed end-stage renal disease. Fifty-five patients had end-stage renal disease resulting from progressive bilateral WT and 118 patients had end-stage renal disease due to other causes, many of whom had WT-associated congenital anomalies. These results suggest that conducting a *WT1* mutation analysis is mandatory in patients with BWT and that affected patients should be carefully followed for a long period, even beyond 10 years after the completion of therapy.

REFERENCES

1. Kubiak R, Gundeti M, Duffy PG, et al. Renal function and outcome following salvage surgery for bilateral Wilms' tumor. J Pediatr Surg 2004;3:1667–1672.
2. Coppes MJ, de Kraker J, Van Dijken PJ, et al. Bilateral Wilms' tumor: Long term survival and some epidemiological features. J Clin Oncol 1989;7:310–315.
3. Shamberger RC, Haase GM, Argani P, et al. Bilateral Wilms' tumors with progressive or nonresponsive disease. J Pediatr Surg 2006;41:652–657.
4. Kumar R, Fitzgerald R, Breatnach F. Conservative surgical management of bilateral Wilms' tumor: Results of the United Kingdom Children's Cancer Study Group. J Urol 1998;160:1450–1453.
5. Hamilton TE, Ritchey ML, Haase GM, et al. The management of synchronous bilateral Wilms tumor: A report of the National Wilms Tumor Study Group. Ann Surg 2011;253:1004–1010.
6. Oue T, Fukuzawa M, Okita H, et al. Outcome of pediatric renal tumor treated using the Japan Wilms Tumor Study-1 (JWiTS-1) protocol: A report from the JWiTS group. Pediatr Surg Int 2009;25:923–929.
7. Shibata R, Hashiguchi A, Sakamoto J, et al. Correlation between a specific Wilms tumour suppressor gene (WT1) mutation and the histological findings in Wilms tumour (WT). J Med Genet 2002;39:e83.
8. Kaplan EL, Meier P. Nonparametric estimation from incomplete observations. J Am Stat Assoc 1958; 53:457–481.
9. Horwitz JR, Ritchey MR, Moksness J, et al. Renal salvage procedure in patients with synchronous bilateral Wilms' tumor: A report from the National Wilms' Tumor Study Group. J Pediatr Surg 1996; 31:1020–1025.
10. Blute ML, Kelalis PP, Offord KP, et al. Bilateral Wilms' tumor. J Urol 1987;138:968–973.
11. Montgomery BT, Kelalis PP, Blute ML, et al. Extended follow up of bilateral Wilms' tumor: Results of the National Wilms' Tumor Study. J Urol 1991;146:514–518.
12. Shearer P, Parham DM, Fontanesi J, et al. Bilateral Wilms' tumor: Review of outcome, associated abnormalities, and late effects in 36 pediatric patients treated at a single institution. Cancer 1993;72: 1422–1426.
13. Madre C, Orbach D, Baudouin V, et al. Hypertension in childhood cancer: A frequent complication of certain tumor sites. J Pediatr Hematol Oncol 2006;28:659–664.
14. Beckwith JB. Precursor lesions of Wilms tumor: Clinical and pathological implications. Med Pediatr Oncol 1993;21:158–168.
15. Sudour H, Audry G, Schleimacher G, et al. Bilateral Wilms tumors (WT) treated with the SIOP 93 protocol in France: Epidemiological survey and patient outcome. Pediatr Blood Cancer 2012;59:57–61.
16. Davidoff AM, Giel DW, Jones DP, et al. The feasibility and outcome of nephron-sparing surgery for children with bilateral Wilms tumor. The St Jude Children's Research Hospital experience: 1999–2006. Cancer 2008;112:2060–2070.
17. Hamilton TE, Ritchey ML, Haase GM, et al. The management of synchronous bilateral Wilms tumor: A report from the National Wilms Tumor Study Group. Ann Surg 2011;253:1004–1010.
18. Lange J, Peterson SM, Takashima JR, et al. Risk factors for end stage renal disease in non-*WT1*-syndromic Wilms tumor. J Urol 2011;186:378–386.
19. Nakadate H, Yokomori K, Watanabe N, et al. Mutations/deletions of the WT1 gene, loss of heterozygosity on chromosome arms 11p and 11q, chromosome ploidy and histology in Wilms' tumors in Japan. Int J Cancer 2001;94:396–400.
20. Haruta M, Arai Y, Sugawara W, et al. Duplication of paternal IGF2 or loss of maternal IGF2 imprinting occurs in half of Wilms tumors with various structural WT1 abnormalities. Genes Chromosomes Cancer 2008;47.
21. Haruta M, Arai Y, Watanabe N, et al. Different incidences of epigenetic but not genetic abnormalities between Wilms tumors in Japanese and Caucasian children. Cancer Sci 2012;103:1129–1135.
22. Breslow NE, Takashima JR, Ritchey ML, et al. Renal failure in the Denys-Drash and Wilms' tumoraniridia syndromes. Cancer Res 2000;60:4030–4032.
23. Breslow NE, Collins AJ, Ritchey ML, et al. End stage renal disease in patients with Wilms' tumor: Results from the National Wilms' Tumor Study Group and the United States Renal Data System. J Urol 2005;174:1972–1975.
24. Peterson SM, Takashima JR, Grivoriev Y, et al. Risk factors for end stage renal disease in non-WT1-syndromic Wilms tumor. J Urol 2011;186:378–386.
25. Diller L, Ghahremani M, Morgan J, et al. Frequency of constitutional mutations in the WT1 gene in patients with Wilms tumors. J Clin Oncol 1998;16:3634–3640.
26. Grigoriev Y, Lange J, Peterson SM, et al. Treatments and outcomes for end stage renal disease following Wilms tumor. Pediatr Nephrol 2012;27:1325–1333.

Tumor and Stem Cell Biology

Cancer Research

Trim32 Facilitates Degradation of MYCN on Spindle Poles and Induces Asymmetric Cell Division in Human Neuroblastoma Cells

Hideki Izumi and Yasuhiko Kaneko

Abstract

Asymmetric cell division (ACD) is a physiologic process during development and tissue homeostasis. ACD produces two unequal daughter cells: one has stem/progenitor cell activity and the other has potential for differentiation. Recent studies showed that misregulation of the balance between self-renewal and differentiation by ACD may lead to tumorigenesis in *Drosophila* neuroblasts. However, it is still largely unknown whether human cancer stem–like cells exhibit ACD or not. Here, using human neuroblastoma cells as an ACD model, we found that MYCN accumulates at spindle poles by GSK-3β phosphorylation during mitosis. In parallel, the ACD-related ubiquitin ligase Trim32 was recruited to spindle poles by CDK1/cyclin B–mediated phosphorylation. Trim32 interacted with MYCN at spindle poles during mitosis, facilitating proteasomal degradation of MYCN at spindle poles and inducing ACD. Trim32 also suppressed sphere formation of neuroblastoma-initiating cells, suggesting that the mechanisms of ACD produce differentiated neuroblastoma cells that will eventually die. Thus, Trim32 is a positive regulator of ACD that acts against MYCN and should be considered as a tumor-suppressor candidate. Our findings offer novel insights into the mechanisms of ACD and clarify its contributions to human tumorigenesis. *Cancer Res; 74(19); 5620–30. ©2014 AACR.*

Introduction

Asymmetric cell division (ACD) is a physiologic process that occurs during development and tissue homeostasis in a large variety of organisms. ACD produces two unequal daughter cells; one has multipotent stem and/or progenitor cell activity and the other has potential for differentiation. Recent ACD studies using model organism systems revealed that the balance between self-renewal and differentiation by ACD is robustly controlled and that misregulation of this balance may lead to tumorigenesis in *Drosophila* neuroblasts (1–3).

Neuroblastoma is one of the major childhood tumors (4–6) and is derived from normal neural crest cells, which serve as multipotent stem cells that differentiate into mature tissues, including peripheral neurons (7). Of the many genetic and biochemical features of neuroblastoma, *MYCN* oncogene amplification has been shown to correlate with an aggressive phenotype and a poor outcome (4–6). Recent studies have shown that *MYCN* shows not only oncogenic activity but also plays a central role in self-renewal growth of normal neural stem and precursor cells (8–12). Although the precise role of MYCN in control of the balance between cell self-renewal and differentiation is still unknown, it is now suspected that neuroblastoma has a cancer stem cell–like property due to aberrant MYCN expression in multipotent neural crest cells (7).

Human neuroblastoma cell lines have a unique property in that, although they show unlimited cell proliferation, they are easily induced to become mature neuronal cells by drugs such as retinoic acids (7). Thus, we considered that a human neuroblastoma cell line is the most suitable system for understanding the mechanism of ACD in human cells because it has both self-renewal and differentiation abilities. In fact, we previously reported that NuMA, one of the conserved ACD-related polarity cues, distributed to one side of the cell cortex during cell division, was detected in many *MYCN*-nonamplified human neuroblastoma cell lines, and that MYCN powerfully induced self-renewal division against ACD in *MYCN*-amplified neuroblastoma cells (13). In this study, we attempted to identify the cellular components that abolish the self-renewal proliferation function by MYCN.

Materials and Methods

Cell lines and transfections

All cell lines except TGW were obtained from the American Type Culture Collection (ATCC). TGW was obtained from Japan Health Science Research Resources Bank, Osaka, Japan. All cell lines have been validated by short tandem repeat analysis. These cell lines were maintained in complete medium [Dulbecco's Modified Eagle Medium, supplemented with 10% fetal bovine serum, penicillin (100 U/mL) and

Division of Cancer Therapeutics, Research Institute for Clinical Oncology, Saitama Cancer Center, Saitama, Japan

Corresponding Authors: Hideki Izumi, Division of Cancer Therapeutics, Research Institute for Clinical Oncology, Saitama Cancer Center, 818 Komuro, Ina, Saitama 362-0806, Japan. Phone: 81-48-722-1111; Fax: 81-48-722-1739; E-mail: hideki@cancer-c.pref.saitama.jp; and Yasuhiko Kaneko, kaneko@cancer-c.pref.saitama.jp

doi: 10.1158/0008-5472.CAN-14-0169

streptomycin (100 μg/mL)] in an atmosphere containing 5% CO_2 at 37°C. For transient knockdown in cells, short interfering RNAs targeting the *GSK-3β* (sc-35527), *Cyclin B* (sc-29284), and *Trim32* (sc-61714) cDNA sequences and control siRNA (sc-37007) were obtained from Santa Cruz Biotechnology. The pCMV, pCMV-*N-myc*, pCMV-*Trim32*, pCMV-*Flag*, and pCMV-*Flag-Trim32* vectors were obtained from Origene Technologies. These siRNAs and the plasmid DNAs were transfected using Oligofectamine 2000 (Invitrogen) according to the manufacturer's instructions. After transfection at 37°C for 6 hours, cells were supplied with complete medium for 24 hours and then analyzed. For constructing MYCN-T58A and Flag-Trim32/3A plasmids, the QuikChange Site-Directed Mutagenesis Kit (#200519-5; Agilent Technologies) and QuikChange Lightning Multi-Site-Directed Mutagenesis Kit (#210515-5, Agilent Technologies), respectively, were used. MG-132 (a proteasome inhibitor, #474790, final 10 μmol/L for 5 hours), BIO (GSK-3 inhibitor-IX, #361556, final 1 μmol/L for 3 hours), and RO-3306 (a Cdk1/cyclin B inhibitor, #217699, final 5 μmol/L for 3 hours) were obtained from Calbiochem Inc.

Sphere-forming assay

Stable transfectants were selected with G418 (800 μg/mL) for 10 days. After G418 selection, 1×10^4 transfectants were plated onto Ultra-low cluster 6-well dishes (Corning), and cultured in SFM [DMEM-F12, 1:1 (Wako)], 50 μg/mL penicillin/streptomycin, 2% B27 supplement (Invitrogen), 1% N-2 supplement (Wako), 25 ng/mL epidermal growth factor (Wako), and 25 ng/mL fibroblast growth factor basic (Wako). Half of the medium was replaced with fresh culture medium every 7 days. Spheres were counted and measured under a microscope with an eyepiece micrometer.

Indirect immunofluorescence

Cells grown on coverslips were briefly washed in PBS three times, and then fixed with 100% methanol for 20 minutes at −20°C. The cells were treated with 1% NP-40 in PBS solution for 10 minutes, and were incubated with blocking solution [15% bovine serum albumin (BSA) in PBS] for 1 hour at 37°C. The cells were then probed with primary antibodies for 1 hour, and antibody–antigen complexes were detected with either Alexa Fluor594– or Alexa Fluor488–conjugated donkey secondary antibody (Molecular Probes, Invitrogen) by incubation for 1 hour at room temperature. The samples were washed three times with PBS after each incubation and then counterstained with 4′,6′-diamidino-2-phenylindole (DAPI). Immunostained cells were examined under a fluorescence microscope (Nikon Eclipse E400) using a 100× objective lens. The fluorescence images were captured with a CCD camera (Leica DFC350FX) and processed with Adobe Photoshop (Adobe Systems). The primary antibodies used were as follows: anti-NuMA antibody (NB500-174; Novus Biologicals), anti-MYCN antibody (sc-53993; Santa Cruz Biotechnology), anti-MYCN antibody (#9405S; Cell Signaling Technology), anti-Trim32 antibody (H00022954-M09; Abnova), anti-Fbxw7 antibody (ab71961; Abcam), anti-Huwe1 antibody (ab70161; Abcam), anti-pericentrin antibody (NB100-68277; Novus Biologicals), anti-centrin 2 antibody (sc-2793R; Santa Cruz Biotechnology), anti-phospho-T58 Myc antibody (ab28842; Abcam), anti-phospho-S62 Myc antibody (ab51156; Abcam), anti-c-Myc antibody (9E10, MA1-980; Thermo Scientific), and anti-Flag antibody (#2368S; Cell Signaling Technology).

Immunoblot and immunoprecipitation analyses

Cells were lysed in SDS/Nonidet P-40 lysis buffer [1% SDS, 1% Nonidet P-40, 50 mmol/L Tris (pH 8.0), 150 mmol/L NaCl, 2 μg/mL leupeptin, 2 μg/mL aprotinin, 1 mmol/L phenylmethylsulfonyl fluoride (PMSF), 5 mmol/L NaF, and 100 μmol/L Na_3VO_4). The lysates were boiled for 5 minutes and then cleared by centrifugation at 15,000 rpm and 4°C. Protein concentration of the supernatant was determined using a BCA Protein Assay Reagent (Pierce). The lysates were further boiled for 5 minutes in sample buffer. Samples were then resolved by SDS-PAGE and transferred onto Immobilon-P (Millipore Corp.) sheets. The blots were first incubated in blocking buffer [5% (w/v) nonfat dry milk in Tris-buffered saline (TBS) plus 0.05% Tween 20] for 1 hour. The blots were then incubated with a primary antibody for 16 hours at 4°C, followed by incubation with a horseradish peroxidase–conjugated secondary antibody for 1 hour at room temperature. The antibody–antigen complex was visualized by ECL-plus chemiluminescence (Amersham Pharmacia Biotech). For immunoprecipitations, cells were lysed in 0.5% Nonidet P-40 lysis buffer. One milligram of lysates was precleared by incubation with 20 μL of protein G- or A-conjugated agarose for 1 hour at 4°C and incubated on a platform shaker for 3 hours with the primary antibody (4 μg) at 4°C. Protein G- or A-conjugated agarose (40 μL of protein) was then added to the lysate, and the mixture was further incubated on a platform shaker for 1 hour at 4°C, spun down, and washed three times in wash buffer [0.1% Nonidet P-40; 50 mmol/L Tris (pH 8.0), 150 mmol/L NaCl, 2 μg/mL leupeptin, 2 μg/mL aprotinin, 1 mmol/L PMSF, 5 mmol/L NaF, and 100 μmol/L Na3VO4). After these washes, proteins bound to the beads were eluted with sample buffer by boiling at 95°C for 5 minutes, separated by SDS-PAGE, and analyzed by immunoblotting. The primary antibodies used were anti-GSK-3β antibody (sc-7291; Santa Cruz Biotechnology), anti-cyclin B antibody (sc-245; Santa Cruz Biotechnology), anti-β-actin antibody (#612656; BD Biosciences), anti-Trim32 antibody (H00022954-M09; Abnova), anti-Trim32 antibody (sc-53993; Santa Cruz Biotechnology), anti-Trim32 antibody (sc-9011; Santa Cruz Biotechnology), anti-MYCN antibody (sc-53993; Santa Cruz Biotechnology), anti-MYCN antibody (sc-791; Santa Cruz Biotechnology), anti-GST antibody (PM013 and MBL), and anti-γ-tubulin monoclonal antibody (clone GTU-88; Sigma).

Measurement of proteasome activity and *in vitro* ubiquitinylation assay

For the measurement of proteasome activity in individual cell lines, the Proteasome Activity Assay Kit (ab107921; Abcam) was used according to the manufacturer's instructions. For ubiquitinylation assay, the lysate from TGW cells was immunoprecipitated by anti-Trim32 antibody, and then an auto-ubiquitinylation kit (#BML-UW0970; Enzo Life Sciences) was used according to the manufacturer's instructions.

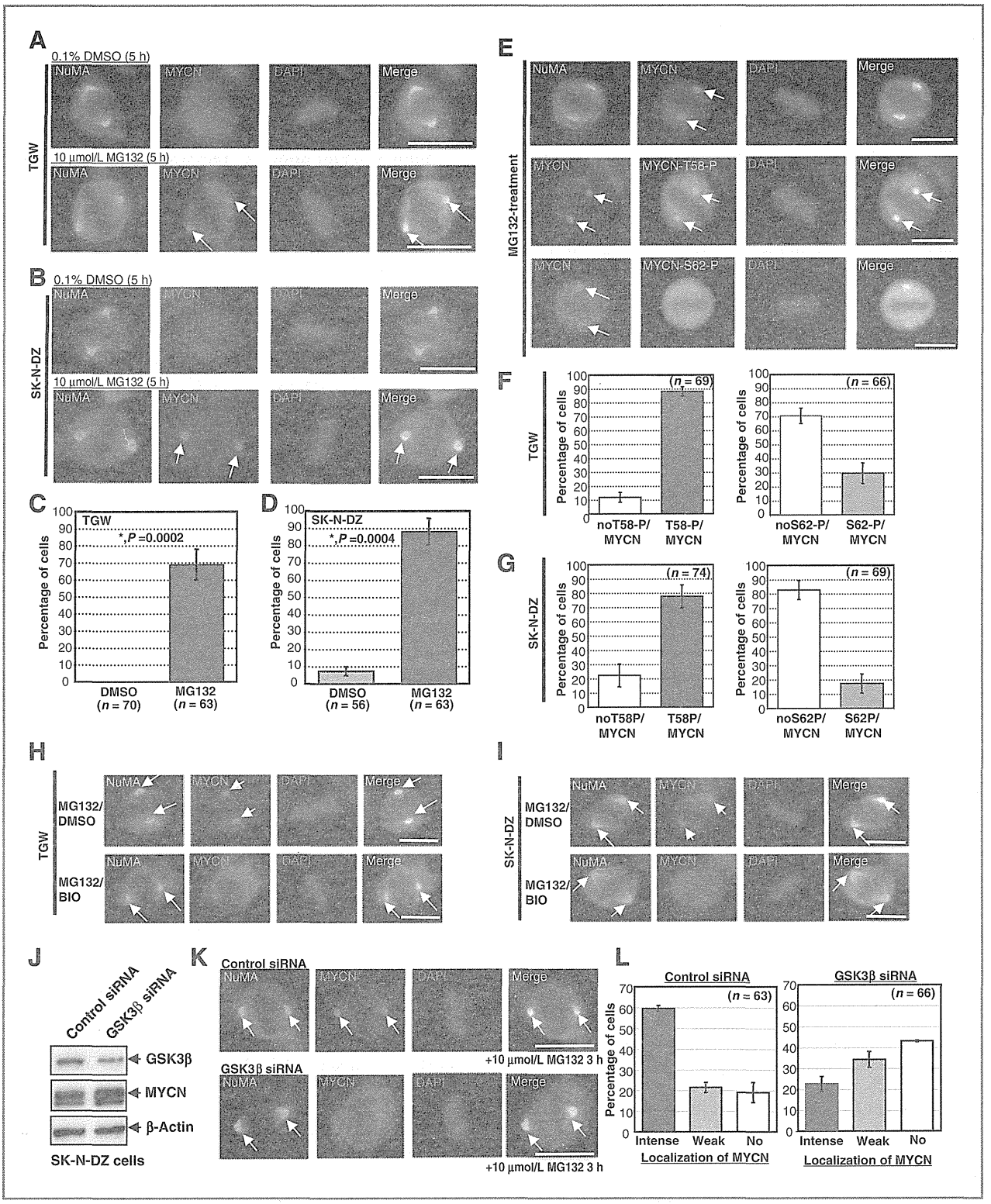

Figure 1. MYCN is localized at spindle poles during mitosis via the GSK-3β phosphorylation signaling pathway. A and B, representative images of accumulation of MYCN protein at spindle poles during mitosis in TGW and SK-N-DZ cells upon exposure to 10 μmol/L MG132 for 5 hours. DMSO (0.1%)-treated cells were used as a control. Spindle pole marker NuMA, green; MYCN, red; DAPI (DNA), blue. Arrows, spindle poles. C and D, percentage of cells with MYCN accumulation at spindle poles in TGW or SK-N-DZ cells. Error bars, SEM from three experiments; $P = 0.0002$ for TGW and $P = 0.0004$ for SK-N-DZ. *Y*-axis shows percentage of cells with MYCN-accumulated spindle poles. E, representative images of phospho-T58-MYCN but not phospho-S62-MYCN accumulation at spindle poles during mitosis in TGW cells. (*Continued on the following page.*)

Statistical analysis

Comparisons of the frequencies of polarity between different groups were carried out using the unpaired Student *t* test, owing to the binary nature of the datasets (asymmetric vs. symmetric). Statistical analysis was performed using a statistical software package (StatView, JMP). Probability values less than 0.05 were considered significant.

Results

MYCN is accumulated at spindle poles during mitosis through GSK-3β phosphorylation signaling

Because ACD is a highlight event during mitosis, we performed immunostaining experiments using *MYCN*-amplified human neuroblastoma cell lines to address where MYCN localized during mitosis. MYCN was present all over the cells and did not localize to any particular organelle (Fig. 1A and B). However, when we treated the cells with a proteasome inhibitor, MG-132, for 5 hours, surprisingly, we found that a large amount of MYCN protein accumulated at spindle poles in TGW and SK-N-DZ cells (Fig. 1A and B). In fact, a significant number of mitotic cells showed MYCN accumulation at spindle poles (Fig. 1C and D). We also attempted the same experiment using other *MYCN*-amplified human neuroblastoma cell lines such as SK-N-BE and CHP-212 (Supplementary Fig. S1A). In these cell lines, MYCN physiologically accumulated at spindle poles during mitosis in a proteasome inhibitor–independent manner. From these results, we speculated that spindle poles are a site of physiologic degradation for MYCN, and detection of MYCN localization at spindle poles depends on the level of endogenous proteasome activity in individual cell lines. Therefore, we measured proteasome activity in these cell lines (Supplementary Fig. S1B). As expected, in the cells with high proteasome activity (TGW and SK-N-DZ), proteasome inhibitor treatment was necessary for the detection of MYCN localization at spindle poles. On the other hand, in the cells with low proteasome activity (SK-N-BE and CHP-212), accumulation of MYCN at spindle poles was physiologically detected without proteasome inhibitor treatment. Thus, spindle poles are an important site for the degradation of MYCN. What about the case for c-MYC protein? We examined whether c-MYC also accumulated at spindle poles during mitosis by using a *c-MYC*--amplified cell line (SK-BR-3) and c-MYC–overexpressed cell lines (HeLa and U251-MG; Supplementary Fig. S2). As a result, c-MYC did not accumulate at spindle poles even when treated with a proteasome inhibitor. Thus, the degradation kinetics of c-MYC differs from that of MYCN, as reported previously (14), and the degradation of MYCN is a unique property during mitosis.

Next, we examined the phosphorylation status of MYCN accumulated at spindle poles. Immunostaining experiments showed that the majority of accumulated MYCN at spindle poles was in the threonine (T) 58-phosphorylated form and the proportion of the S62-phosphorylated form was very low (Fig. 1E–G, and Supplementary Fig. S3). Because GSK-3β is known to phosphorylate MYCN at T58 (6, 15), we treated the cells with MG-132 plus GSK-3 kinase inhibitor, BIO. Immunostaining experiments revealed that the proportion of accumulated MYCN significantly decreased (Fig. 1H and I and Supplementary Fig. S4). Therefore, we speculated that GSK-3β phosphorylation signaling might recruit MYCN to spindle poles. To address this point precisely, we silenced GSK-3β expression with siRNA, treated with MG-132 for 3 hours, and then performed an immunostaining experiment (Fig. 1J and K). As expected, the proportion of MYCN accumulation at spindle poles was reduced despite high MYCN protein levels (Fig. 1J–L). These findings provide the evidence that GSK-3β phosphorylation signaling recruits MYCN to spindle poles in human neuroblastoma cells.

Trim32 is recruited to spindle poles during mitosis through Cdk1/cyclin B phosphorylation signaling

Because it is now known that proteasome is involved in MYCN/c-MYC degradation, we searched for MYC-related ubiquitin ligases such as Trim32 (16, 17), Fbxw7 (18, 19), and Huwe1 (20) that facilitate the degradation of MYCN in proteasome, by localizing at spindle poles during mitosis. We found that Trim32 localized at spindle poles during mitosis, but not in interphase (Fig. 2A). On the other hand, other MYC-related ubiquitin ligases such as Fbxw7 and Huwe1 did not localize at spindle poles during mitosis (Supplementary Fig. S5A and S5B). Thus, Trim32 is a plausible ubiquitin ligase for MYCN degradation. As mentioned above, Trim32 does not localize at centrosomes in interphase, but localizes at spindle poles during mitosis. In addition, it is reported that Trim32 is phosphorylated at its serine residues (S328, S335, and S339) by Cdk1/cyclin B (21, 22). Therefore, we speculated that phosphorylation of Cdk1/cyclin B is important for Trim32 to localize at spindle poles. To test this hypothesis, we treated the cells with a low dose (5 μmol/L) of a Cdk1/cyclin B inhibitor, RO-3306 (Supplementary Fig. S6), and then performed immunostaining. Interestingly, RO-3306 treatment abolished the spindle pole localization of Trim32 (Fig. 2B and C and Supplementary Fig. S7). Therefore, we next silenced cyclin B expression with siRNA (Fig. 2D). Knockdown of cyclin B caused displacement of Trim32 from spindle poles (Fig. 2E and F). In addition, we constructed a phosphorylation-deficient mutant

(*Continued.*) MYCN, red; phospho-T58-MYCN or phospho-S62-MYCN, green; DAPI (DNA), blue. Arrows, spindle poles. F and G, percentage of cells with phosphorylated or unphosphorylated MYCN at spindle poles in TGW and SK-N-DZ cells. Error bars, SEM from three experiments. H and I, representative images of MYCN accumulation at spindle poles during mitosis in TGW and SK-N-DZ cells upon exposure to 10 μmol/L MG132 plus 0.1% DMSO or 1 μmol/L BIO for 3 hours. NuMA, green; MYCN, red; DAPI (DNA), blue. Arrows, spindle poles. J, immunoblot of GSK-3β and MYCN expression in SK-N-DZ cells transfected with control siRNA or *GSK3β* siRNA. Immunoblot of β-actin served as a loading control. K, representative images of MYCN accumulation at spindle poles during mitosis in SK-N-DZ cells transfected with control siRNA or *GSK3β* siRNA. After transfection of siRNAs, the cells were treated with 10 μmol/L MG132 for 3 hours. NuMA, green; MYCN, red; DAPI (DNA), blue. Arrows, spindle poles. L, percentage of cells with MYCN accumulation at spindle poles in SK-N-DZ cells transfected with control siRNA or *GSK3β* siRNA. Error bars, SEM from three experiments. Localization statuses of MYCN on spindle poles were categorized into three types (intense, weak, or no localization). Scale bars, 10 μm.

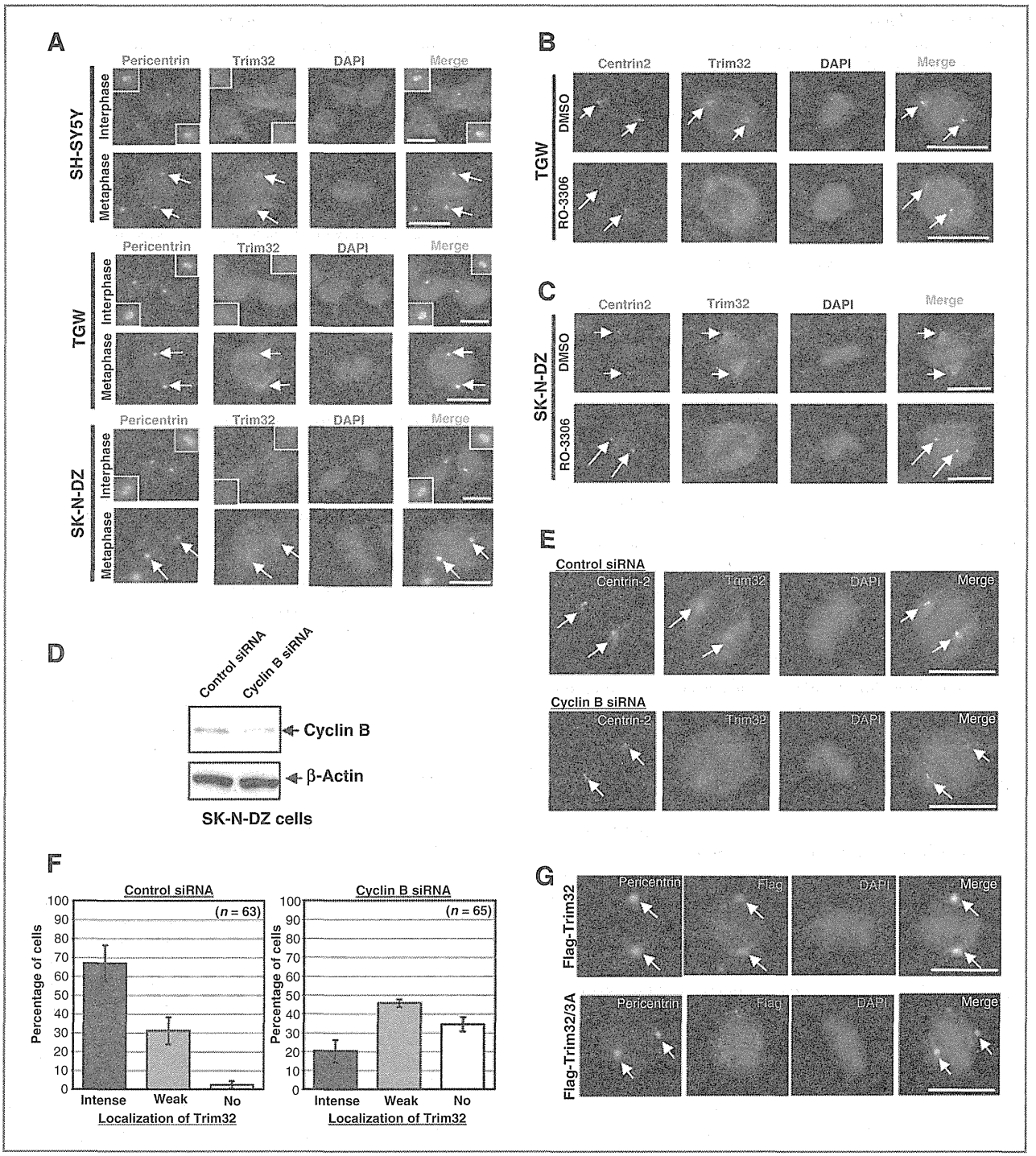

Figure 2. Trim32 is recruited to spindle poles during mitosis through Cdk1/cyclin B phosphorylation signaling. A, representative images of localization of Trim32 to spindle poles during mitosis but not in interphase in SH-SY5Y, TGW, and SK-N-DZ cells. Centrosome marker pericentrin, green; Trim32, red; DAPI (DNA), blue. Arrows, spindle poles. B and C, representative images of Trim32 localization to spindle poles during mitosis in TGW and SK-N-DZ cells upon exposure to 5 μmol/L RO-3306 for 3 hours. DMSO (0.1%)-treated cells were used as a control. Centrosome (centriole) marker centrin-2, is green; Trim32, red; DAPI (DNA), blue. Arrows, spindle poles. D, immunoblot of cyclin B expression in SK-N-DZ cells transfected with control siRNA or *Cyclin B* siRNA. Immunoblot of β-actin served as a loading control. E, representative images of Trim32 localization to spindle poles during mitosis in SK-N-DZ cells transfected with control siRNA or *Cyclin B* siRNA. Centrin-2, green; Trim32, red; DAPI (DNA), blue. Arrows, spindle poles. F, percentage of cells with Trim32 localization to spindle poles in SK-N-DZ cells transfected with control siRNA or *Cyclin B* siRNA. Error bars, SEM from three experiments. Localization statuses of Trim32 at spindle poles were categorized into three types (intense, weak, or no localization). G, representative images of Flag-Trim32 or Flag-Trim32/3A localization to spindle poles during mitosis in SK-N-DZ cells transfected with *Flag-Trim32* or *Flag-trim32/3A* expression vector. Pericentrin, green; Flag, red; DAPI (DNA), blue. Arrows, spindle poles. Flag-Trim32 localizes to spindle poles, but Flag-Trim32/3A does not. Scale bars, 10 μm.

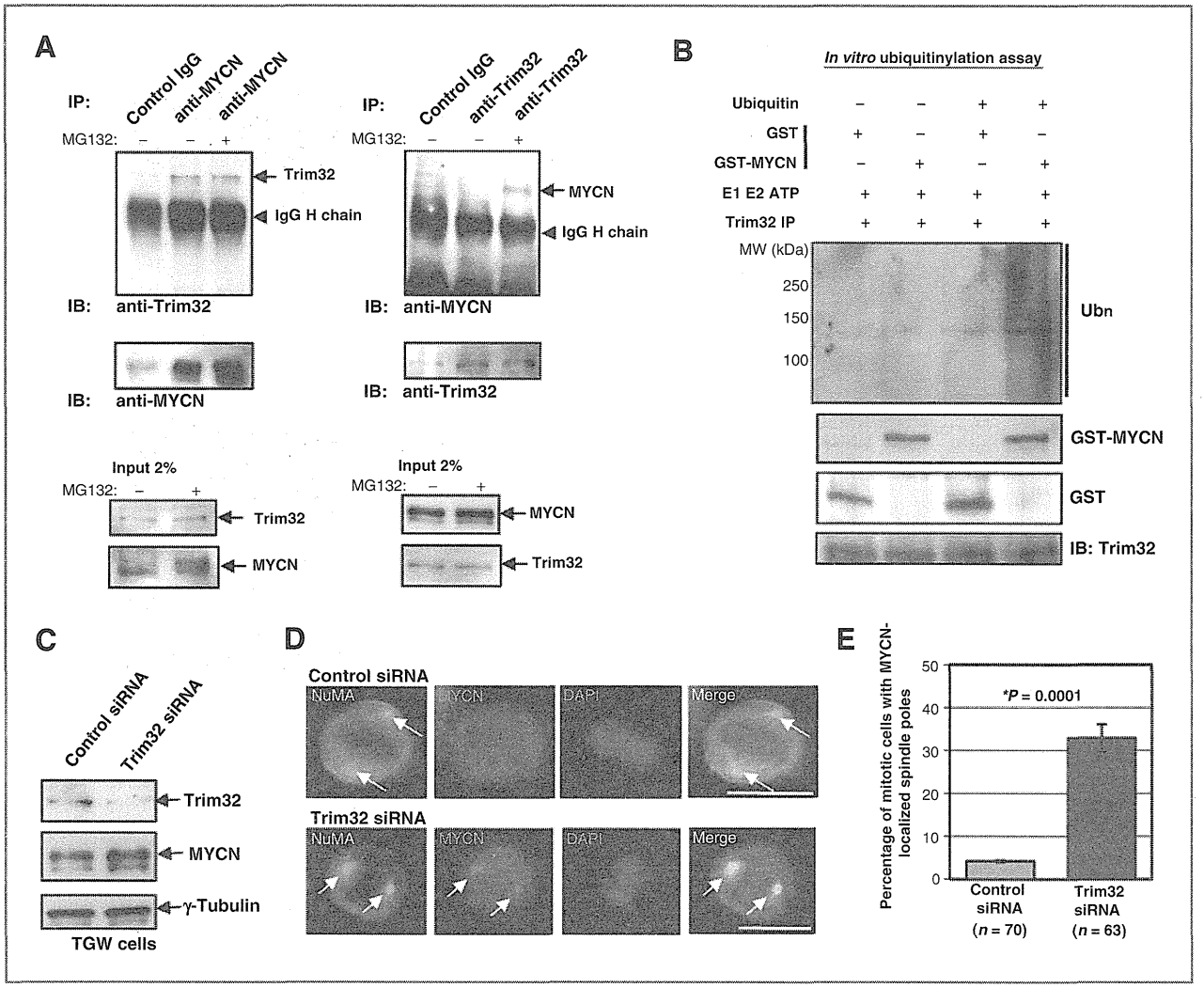

Figure 3. MYCN is a physiologic substrate of Trim32 ubiquitin ligase. A, one milligram of cell lysate from TGW cells was immunoprecipitated with an anti-MYCN antibody. As a control, immunoprecipitates with preimmune mouse immunoglobulin-G (IgG) were used. The immunoprecipitates were then subjected to immunoblotting using an anti-Trim32 antibody (left). Conversely, 1 mg of cell lysate was immunoprecipitated with an anti-Trim32 antibody, and the immunoprecipitates were subjected to immunoblotting using an anti-MYCN antibody. As a control, immunoprecipitates with preimmune mouse IgG were used (right). B, Trim32 directly ubiquitinylates MYCN *in vitro*. Trim32 immunoprecipitates from TGW cells were mixed with GST or recombinant GST-MYCN with or without ubiquitin, and an *in vitro* ubiquitylation assay was performed. C, immunoblot of Trim32 and MYCN expression in TGW cells transfected with control siRNA or *Trim32* siRNA. Immunoblot of γ-tubulin served as a loading control. D, representative images of MYCN localization to spindle poles during mitosis in TGW cells transfected with control siRNA or *Trim32* siRNA. NuMA, green; MYCN, red; DAPI (DNA), blue. Arrows, spindle poles. Scale bars, 10 μm. E, percentage of cells with MYCN-localized spindle poles in TGW cells transfected with control siRNA or *Trim32* siRNA. Error bars, SEM from three experiments. *Y*-axis, percentage of mitotic cells with MYCN-localized spindle poles.

of Trim32 [Trim32-S328A, S335A, and S339A (Trim32/3A)], and then transfected this mutant plasmid into the cells. As expected, the phosphorylation-deficient mutant of Trim32 did not localize at spindle poles during mitosis, whereas the wild-type Trim32 did. Thus, the Cdk1/cyclin B phosphorylation signal recruits Trim32 to spindle poles (Fig. 2G).

MYCN is a physiologic substrate of Trim32 ubiquitin ligase

We next examined whether Trim32 interacts with MYCN. Immunostaining experiments showed that Trim32 colocalized with MYCN at spindle poles under proteasome inhibitor treatment (Supplementary Fig. S8A and S8B). Therefore, the cell lysate from *MYCN*-amplified cells was immunoprecipitated using an anti-MYCN antibody, and then the immunoprecipitates were blotted using an anti-Trim32 antibody. As a result, a Trim32 band was detected (Fig. 3A). Alternatively, the lysate was immunoprecipitated using an anti-Trim32 antibody, and then the immunoprecipitates were blotted using an anti-MYCN antibody. Interestingly, an MYCN band was detected only in the proteasome inhibitor (MG-132)–treated sample, but not in the untreated one (Fig. 3A). This result strongly suggests that Trim32 interacts with MYCN *in vivo*, and then rapidly ubiquitinylates MYCN protein, followed by degradation

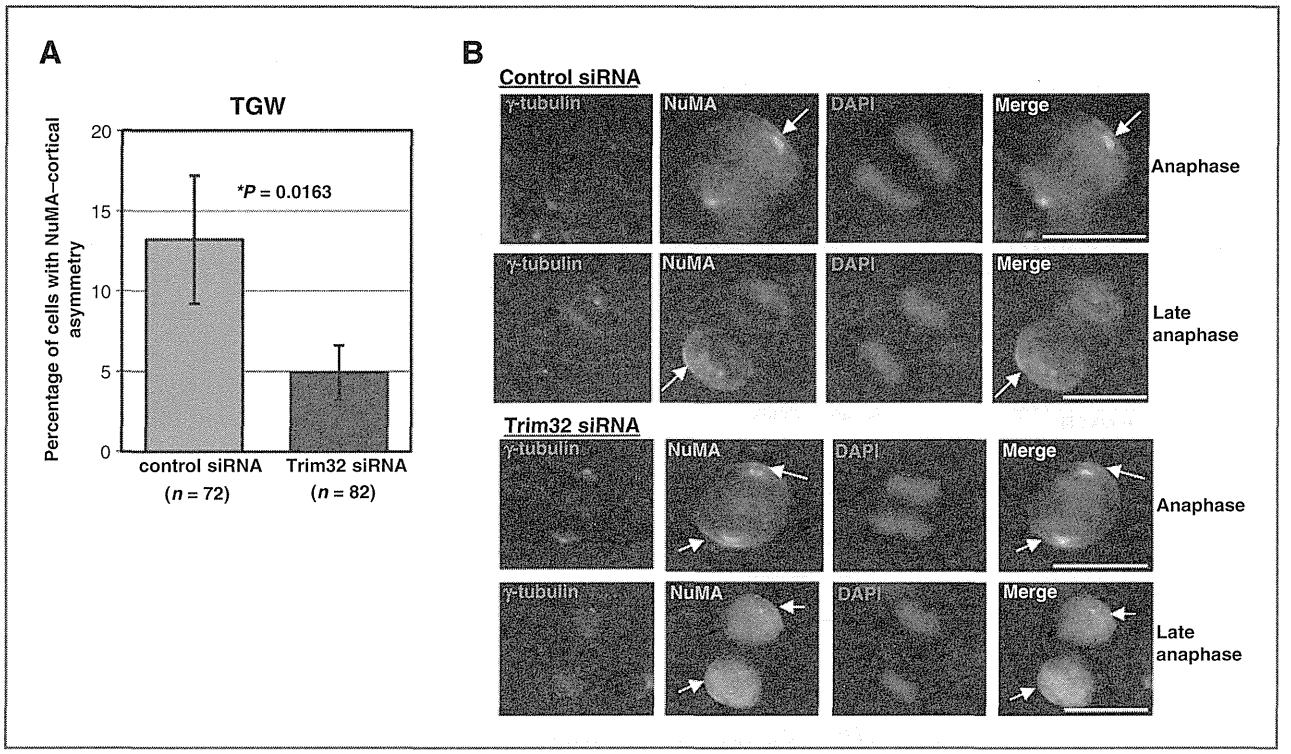

Figure 4. Trim32 may be an inducer of ACD against MYCN function. TGW cells show approximately 10% NuMA cortex based–asymmetric cell division (N-ACD). A, TGW cells were transfected with *Trim32* siRNA, and we then counted the percentage of NuMA-ACD cells with or without Trim32 knockdown. A, percentage of TGW cells with NuMA-ACD transfected with control or *Trim32* siRNA. Error bars, SEM from three experiments; $P = 0.0163$. B, representative images of NuMA-ACD in TGW with control siRNA or *Trim32* siRNA. Cell cortex marker NuMA, green; γ-tubulin, red; DAPI (DNA), blue. Arrows, NuMA-cortex. Percentage of TGW cells with NuMA-ACD was significantly reduced by knockdown of Trim 32.

via the proteasome system. We also addressed whether Trim32 interacts with MYCN in a T58 phosphorylation–dependent manner. We transfected MYCN (wild-type) or MYCN-T58 phosphorylation-deficient mutant (MYCN-T58A) into *MYCN*-nonamplified cells (SH-SY5Y), and then performed an immunoprecipitation experiment. As a result, Trim32 interacted with MYCN in a phosphorylation-independent manner (Supplementary Fig. S9), suggesting that phosphorylation is dispensable for MYCN to bind Trim32, and that spindle poles are important sites for the interaction between Trim32 and MYCN because both proteins localize to spindle poles during mitosis. Moreover, we attempted an *in vitro* ubiquitinylation assay to examine whether Trim32 ubiquitinylates MYCN. Trim32 was immunoprecipitated by an anti-Trim32 antibody, and then E1, E2 ubiquitin ligase complex, ATP, ubiquitin, and GST or GST-MYCN were added in the Trim32 immunoprecipitates. The result clearly showed that GST-MYCN was polyubiquitinylated by Trim32 *in vitro* (Fig. 3B). In addition, we addressed the ubiquitinylation activity of Trim32 during mitosis. As a result, the ubiquitin ligase of Trim32 was shown to be active during both interphase and mitosis (Supplementary Fig. S10).

Next, when we silenced Trim32 expression with siRNA, as expected, the immunoblotting experiment showed that the MYCN protein level increased (Fig. 3C). In addition, importantly, in the Trim32-knockdown cells, an immunostaining experiment revealed that MYCN protein significantly accumulated at spindle poles without proteasome inhibitor treatment (Fig. 3D and E). These results strongly suggest that MYCN is a physiologic substrate of Trim32 in human neuroblastoma cells.

We recently reported that, while *MYCN*-nonamplified neuroblastoma cells showed NuMA cortex-based asymmetric cell division (NuMA-ACD) at a high frequency (~30%), *MYCN*-amplified cells showed NuMA-ACD at a low frequency (3% to 10%; ref. 13). Among *MYCN*-amplified cells, TGW cells showed NuMA-ACD at approximately 10% (13). Therefore, we examined the proportion of NuMA-ACD with or without Trim32 knockdown. The results showed that the proportion of NuMA-ACD was significantly reduced in Trim32-knockdown TGW cells (Fig. 4A and B), suggesting that Trim32 might be an inducer of ACD against MYCN.

We subsequently transfected the *Trim32* or *Trim32/3A* expression vector into the *MYCN*-amplified cells (SK-N-DZ) to determine whether Trim32 and its mutant have ubiquitinylation function. The results showed that Trim32/3A as well as Trim32 had ubiquitinylation activity because MYCN protein level decreased in both Flag-Trim32- and Flag-Trim32/3A–transfected cells (Fig. 5A). However, importantly, the proportion of Flag-Trim32/3A cells with aggresome significantly increased compared with that of Flag-Trim32 cells (Fig. 5B). It is known that aggresomes represent a misconnection between ubiquitin ligase and other components of the proteasome complex (23–27). These results suggest that, although the

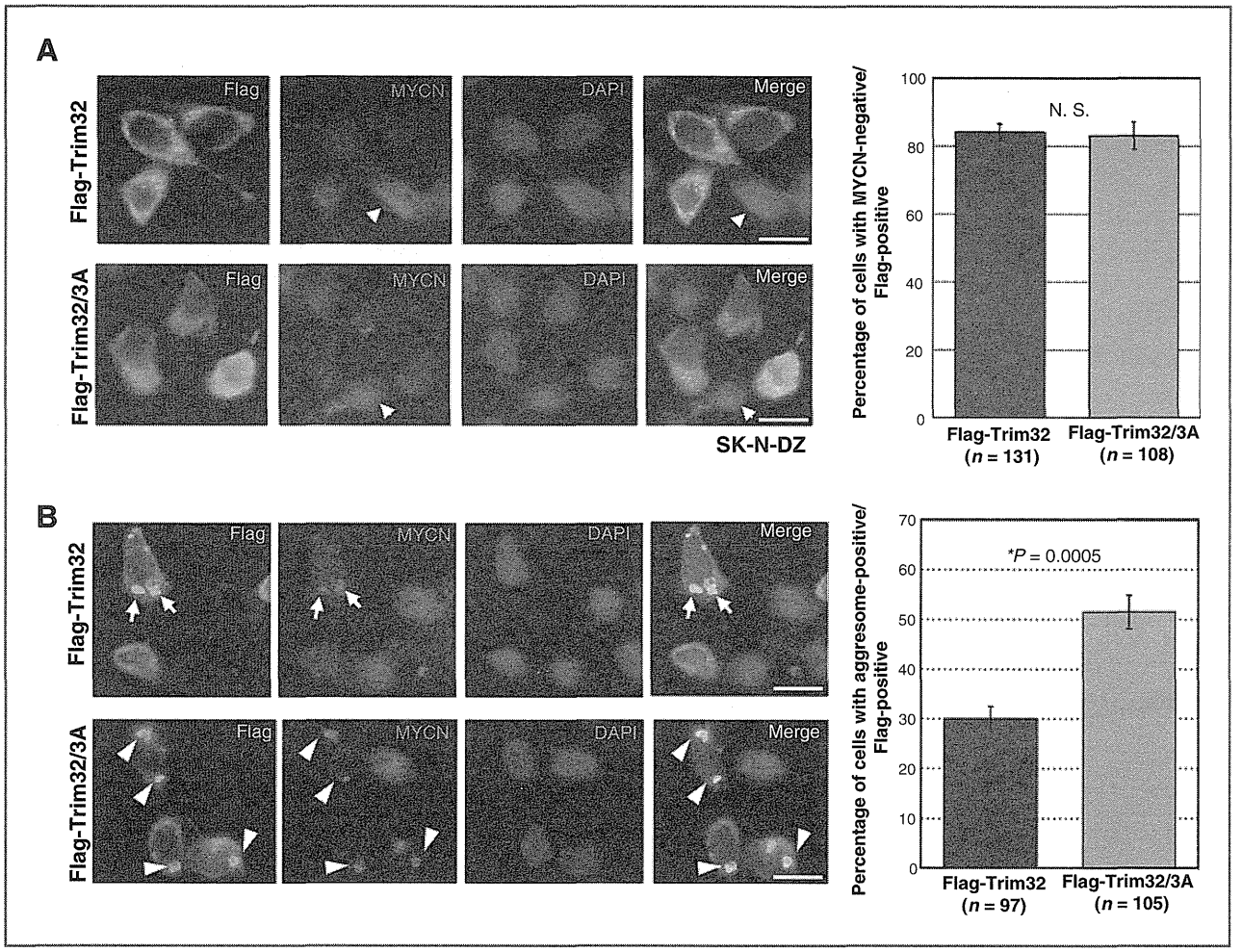

Figure 5. Trim32/3A has ubiquitinylation activity for MYCN, but induces aggresome. A, representative images of Flag- and MYCN-stained SK-N-DZ cells transfected with the *Flag-Trim32* or *Flag-Trim32/3A* expression vector. Flag, green; MYCN, red; DAPI (DNA), blue. Arrowheads, untransfected cells. While MYCN signals were detected in untransfected cells, MYCN signals were not detected in Flag-Trim32- and Flag-Trim32/3A-transfected cells. Percentage of MYCN-negative/Flag-positive cells is shown on the right side. Error bars, SEM from three experiments. B, representative images of Flag- and MYCN-stained SK-N-DZ cells transfected with the *Flag-trim32* or *Flag-Trim32/3A* expression vector. Flag, green; MYCN, red; DAPI (DNA), blue. Arrows, aggresomes in Flag-Trim32-transfected cells. Arrowheads, aggresomes in Flag-Trim32/3A–transfected cells. Percentage of aggresome-positive cells is shown in right. Error bars, SEM from three experiments; $P = 0.0005$.

Trim32/3A mutant still has ubiquitinylation activity for MYCN, it does not have reliable signaling interaction for the proteasome system.

Trim32 suppresses sphere-forming ability in human neuroblastoma cells

We also transfected the *Trim32* or *Trim32/3A* expression vector into *MYCN*-amplified cells (SK-N-DZ) and performed the sphere-forming assay to determine whether Trim32 affects the self-renewal growth of neuroblastoma cells. After selection of transfectants, each transfectant was plated onto ultra-low attachment dishes and, after 7 days, the large spheres of $\geq$100 μm in diameter were counted (Fig. 6A). Interestingly, SK-N-DZ transfected with a control vector showed significantly higher numbers of large spheres than the Flag-Trim32–transfected cells (Fig. 6A and B). This strongly suggests that Trim32 has the ability to block self-renewal division (symmetric cell division) of cancer-initiating/stem cells. In addition, the Flag-Trim32/3A–transfected cells somewhat recovered the ability of sphere formation compared with the Flag-Trim32–transfected cells (Fig. 6A and B). These findings suggest that spindle pole localization of Trim32 may be important for blocking self-renewal growth in neuroblastoma cells.

Trim32 induces ACD in human neuroblastoma cells

We finally transfected the *Trim32* or *Trim32/3A* expression vector into *MYCN*-amplified cells (SK-N-DZ; Fig. 7A), and examined the status of ACD by immunostaining (Fig. 7B). As reported previously (13), SK-N-DZ rarely showed NuMA-ACD (~3%). However, in Trim32-transfected cells, MYCN protein level decreased and complete ACD (opposite distributions of NuMA and Trim32) was detected (complete

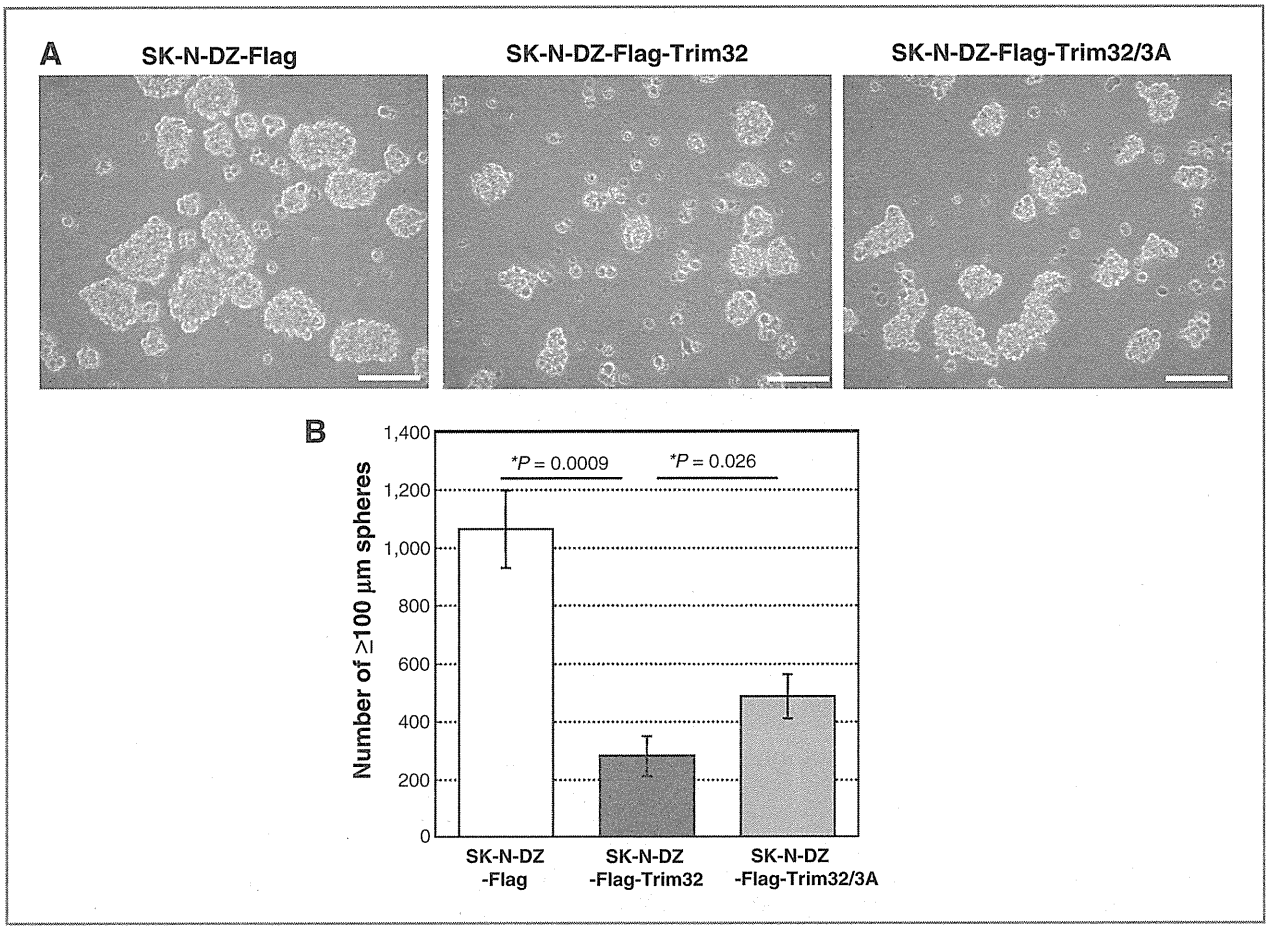

Figure 6. Trim32 suppresses sphere formation in human neuroblastoma cells. A, representative images of sphere formation in Flag (control)-transfected, Flag-Trim32–transfected, and Flag-Trim32/3A–transfected SK-N-DZ after 7 days. Scale bars, 100 μm. B, numbers of spheres of ≥100 μm in each transfectant. Error bars, SEM from triplicate experiments. The numbers of spheres of ≥100 μm were lower in Flag-Trim32–transfected cells ($P = 0.0009$) and in Flag-Trim32/32A–transfected cells ($P = 0.026$) than in Flag (control)-transfected ones.

ACD; Fig. 7B and C). We additionally found ACD, in which Trim32 was oppositely distributed from MYCN at the end of cell division (Supplementary Fig. S11). We believe that this ACD status occurs in a neuroblastoma-specific manner. In Trim32-transfected cells, it was also detected that both NuMA and Trim32 localized to the same side of the daughter cell during anaphase (Fig. 7B). We termed this aberrant ACD "sympatric ACD." Although it is unknown why sympatric ACD was detected, correct distribution of other ACD-related components might be necessary for establishing complete ACD. In Trim32/3A-transfected cells, NuMA-ACD was detected but Trim32 distribution was not asymmetric (Fig. 7B and C). We also performed the transfection of the Trim32/3A vector with *MYCN* shRNA into SK-N-DZ cells (Supplementary Fig. S12A). Interestingly, in Trim32/3A-transfected and *MYCN*-knockdown cells, the percentage of NuMA-ACD cells significantly increased (Supplementary Fig. S12B). This result indicates that MYCN interferes with NuMA-ACD. Together, these results suggest that spindle pole localization of Trim32 may be important for both degradation of MYCN and reliable induction of complete ACD (Fig. 7D).

Discussion

In the present study, we found that Trim32 may be an inducer of ACD in our human neuroblastoma cell system. Recent studies showed that human neuroblastoma cells contain tumor-initiating cells whose phenotype resembles cancer stem cells, including features such as self-renewal, induction of multilineage cell differentiation, and high drug efflux capacity (7, 24). ACD is another important characteristic of cancer stem cells, and may cause tumor cell heterogeneity. Because Trim32 degrades MYCN, produces differentiated neuroblastoma cells that will eventually die, and suppresses sphere formation, we consider it to be a tumor suppressor in neuroblastoma. In fact, a public microarray database (R2) for human neuroblastoma using 88 clinical samples showed that patients with high Trim32 expression in neuroblastoma tumors had better relapse-free survival than those with low expression ($P = 0.05$; Supplementary Fig. S13). Therapies enhancing Trim32 activity may, thus, lead to a cure of refractory neuroblastoma with *MYCN* amplification.

In this study, although the forced expression of Trim32 targeted MYCN for degradation in *MYCN*-amplified

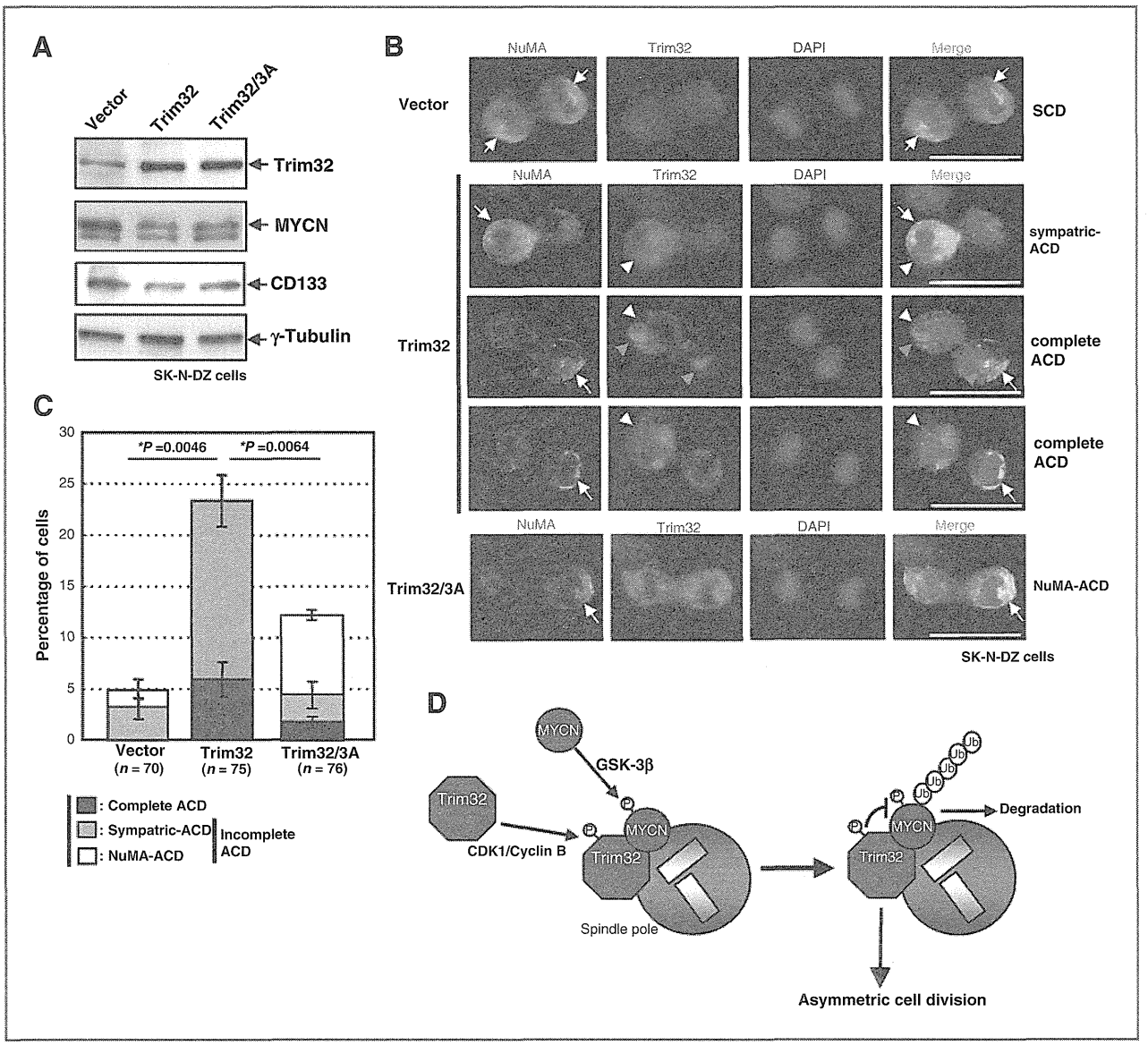

Figure 7. Trim32 induces ACD in human neuroblastoma cells. A, immunoblot of Trim32, MYCN, and CD133 (a putative neural stem cell marker) expression in SK-N-DZ cells transfected with the *Trim32* or *Trim32/3A* expression vector. Immunoblot of γ-tubulin served as a loading control. B, representative images of ACD during anaphase in SK-N-DZ cells transfected with the *Trim32* or *Trim32/3A* expression vector. Cell cortex marker NuMA, green; Trim32, red; DAPI (DNA), blue. SCD, symmetric cell division; NuMA-ACD, NuMA-cortex–based ACD; complete ACD, cell division in which NuMA and Trim32 were distributed at opposite ends of a dividing cell; and sympatric ACD, cell division in which NuMA and Trim32 were distributed at the same end of a dividing cell. Arrows, NuMA cortex; arrowheads, Trim32 distribution; red arrowheads, spindle poles. Scale bars, 10 μm. C, percentage of ACD in SK-N-DZ cells transfected with the *Trim32* or *Trim32/3A* expression vector. Error bars, SEM from three experiments. Complete ACD is more frequent in Trim32-transfected cells than in control vector–transfected cells ($P = 0.0046$) or in Trim32/3A–transfected ones ($P = 0.0064$). D, a schematic model of Trim32-mediated ACD in *MYCN*-amplified human neuroblastoma cells.

neuroblastoma cells, we found that Trim32 also localized at spindle poles even in *MYCN*-nonamplified neuroblastoma cells (Fig. 2A, SH-SY5Y cells). This result suggests that Trim32 has not only ubiquitinylation activity for MYCN but may also have other functions. For example, Trim32 is known to function in the translation of mRNAs and to activate microRNAs, such as *let-7* (17). Thus, activation of microRNAs and translation of cell fate–related mRNAs by Trim32 might also be necessary for establishing complete ACD in neuroblastoma cells.

Spindle poles are organelles that ensure reliable segregation of chromosomes during mitosis. Our results show that the spindle pole localization of Trim32 itself may also be important for the suppression of self-renewal growth and the establishment of asymmetric cell polarity during mitosis. It is also known that spindle orientation and asymmetric segregation of cell-fate determinants are important for the establishment of ACD (3). Our results suggest that the spindle pole–associated ubiquitin–proteasome system is also indispensable for ACD. In fact, it is

known that proteasome localizes to centrosomes/spindle poles and functions for cell homeostasis in many mammalian cells (25, 26, 28). In addition, some proteasome components are known to segregate asymmetrically during mitosis in T lymphocytes (29) and human pancreatic cancer cells (30). Thus, we believe that the ubiquitin–proteasome system may largely contribute to the reliable establishment of ACD.

In summary, we showed here that human neuroblastoma cell lines are a very suitable model system for analyzing the mechanism of ACD in human cells. Our study may also provide new therapeutic clues for targeting cancer stem cells.

Disclosure of Potential Conflicts of Interest

No potential conflicts of interests were disclosed.

Authors' Contributions

Conception and design: H. Izumi, Y. Kaneko
Development of methodology: H. Izumi
Acquisition of data (provided animals, acquired and managed patients, provided facilities, etc.): H. Izumi
Analysis and interpretation of data (e.g., statistical analysis, biostatistics, computational analysis): H. Izumi Y. Kaneko
Writing, review and/or revision of the manuscript: H. Izumi, Y. Kaneko
Administrative, technical or material support (i.e., reporting or organizing data, constructing databases): H. Izumi, Y. Kaneko
Study supervision: H. Izumi, Y. Kaneko

Acknowledgments

The authors thank Drs. M. Haruta and Y. Yamaguchi for excellent research support, K. Ono and H. Odagawa for technical assistance, and K. Ogawa and K. Mihashi for secretarial assistance. The authors also thank their laboratory members for continuous encouragement.

Grant Support

This work was supported in part by Grants-in-Aid for Scientific Research from the Ministry of Education, Science, Sports and Culture of Japan and the Kawano Masanori Memorial Foundation for the Promotion of Pediatrics, Japan.

The costs of publication of this article were defrayed in part by the payment of page charges. This article must therefore be hereby marked *advertisement* in accordance with 18 U.S.C. Section 1734 solely to indicate this fact.

Received January 23, 2014; revised June 10, 2014; accepted July 9, 2014; published OnlineFirst August 6, 2014.

References

1. Basto R, Brunk K, Vinadogrova T, Peel N, Franz A, Khodjakov A, et al. Centrosome amplification can initiate tumorigenesis in flies. Cell 2008;133:1032–42.
2. Castellanos E, Dominguez P, Gonzalez C. Centrosome dysfunction in Drosophila neural stem cells causes tumors that are not due to genome instability. Curr Biol 2008;18:1209–14.
3. Knoblich JA. Asymmetric cell division: recent developments and their implications for tumour biology. Nat Rev Mol Cell Biol 2010;11:849–60.
4. Brodeur GM. Neuroblastoma: biological insights into a clinical enigma. Nat Rev Cancer 2003;3:203–16.
5. Schwab M, Westermann F, Hero B, Berthold F. Neuroblastoma: biology and molecular and chromosomal pathology. Lancet Oncol 2003;4:472–80.
6. Huang M, Weiss WA. Neuroblastoma and MYCN. Cold Spring Harb Perspect Med 2013;3:a014415.
7. Ross RA, Spengler BA. Human neuroblastoma stem cells. Semin Cancer Biol 2007;17:241–7.
8. Knoepfler PS, Cheng PF, Eisenman RN. N-myc is essential during neurogenesis for the rapid expansion of progenitor cell populations and the inhibition of neuronal differentiation. Genes Dev 2002;16:2699–712.
9. Mahller YY, Williams JP, Baird WH, Mitton B, Grossheim J, Saeki Y, et al. Neuroblastoma cell lines contain pluripotent tumor initiating cells that are susceptible to a targeted oncolytic virus. PLoS ONE 2009;4:e4235.
10. Cotterman R, Knoepfler PS. N-Myc regulates expression of pluripotency genes in neuroblastoma including lif, klf2, klf4, and lin28b. PLoS ONE 2009;4:e5799.
11. Nakagawa M, Takizawa N, Narita M, Ichisaka T, Yamanaka S. Promotion of direct reprogramming by transformation-deficient Myc. Proc Natl Acad Sci U S A 2010;107:14152–7.
12. Chappell J, Dalton S. Roles for MYC in the establishment and maintenance of pluripotency. Cold Spring Harb Perspect Med 2013;3:a014381.
13. Izumi H, Kaneko Y. Evidence of asymmetric cell division and centrosome inheritance in human neuroblastoma cells. Proc Natl Acad Sci U S A 2012;109:18048–53.
14. Popov N, Schulein C, Jaenicke LA, Eilers M. Ubiquitylation of the amino terminus of Myc by SCF(beta-TrCP) antagonizes SCF(Fbw7)-mediated turnover. Nat Cell Biol 2010;12:973–81.
15. Swartling FJ. Myc proteins in brain tumor development and maintenance. Ups J Med Sci 2012;117:122–31.
16. Betschinger J, Mechtler K, Knoblich JA. Asymmetric segregation of the tumor suppressor brat regulates self-renewal in Drosophila neural stem cells. Cell 2006;124:1241–53.
17. Schwamborn JC, Berezikov E, Knoblich JA. The TRIM-NHL protein TRIM32 activates microRNAs and prevents self-renewal in mouse neural progenitors. Cell 2009;136:913–25.
18. Yada M, Hatakeyama S, Kamura T, Nishiyama M, Tsunematsu R, Imaki H, et al. Phosphorylation-dependent degradation of c-Myc is mediated by the F-box protein Fbw7. EMBO J 2004;23:2116–25.
19. Welcker M, Orian A, Jin J, Grim JE, Harper JW, Eisenman RN, et al. The Fbw7 tumor suppressor regulates glycogen synthase kinase 3 phosphorylation-dependent c-Myc protein degradation. Proc Natl Acad Sci U S A 2004;101:9085–90.
20. Zhao X, Heng JI, Guardavaccaro D, Jiang R, Pagano M, Guillemot F, et al. The HECT-domain ubiquitin ligase Huwe1 controls neural differentiation and proliferation by destabilizing the N-Myc oncoprotein. Nat Cell Biol 2008;10:643–53.
21. Dephoure N, Zhou C, Villen J, Beausoleil SA, Bakalarski CE, Elledge SJ, et al. A quantitative atlas of mitotic phosphorylation. Proc Natl Acad Sci U S A 2008;105:10762–7.
22. Olsen JV, Vermeulen M, Santamaria A, Kumar C, Miller ML, Jensen LJ, et al. Quantitative phosphoproteomics reveals widespread full phosphorylation site occupancy during mitosis. Sci Signal 2010;3:ra3.
23. Fuentealba LC, Eivers E, Geissert D, Taelman V, De Robertis EM. Asymmetric mitosis: Unequal segregation of proteins destined for degradation. Proc Natl Acad Sci U S A 2008;105:7732–7.
24. Wojcik C, DeMartino GN. Intracellular localization of proteasomes. Int J Biochem Cell Biol 2003;35:579–89.
25. Wigley WC, Fabunmi RP, Lee MG, Marino CR, Muallem S, DeMartino GN, et al. Dynamic association of proteasomal machinery with the centrosome. J Cell Biol 1999;145:481–90.
26. Fabunmi RP, Wigley WC, Thomas PJ, DeMartino GN. Activity and regulation of the centrosome-associated proteasome. J Biol Chem 2000;275:409–13.
27. Ehrhardt AG, Sluder G. Spindle pole fragmentation due to proteasome inhibition. J Cell Physiol 2005;204:808–18.
28. Puram SV, Kim AH, Park HY, Anckar J, Bonni A. The ubiquitin receptor S5a/Rpn10 links centrosomal proteasomes with dendrite development in the mammalian brain. Cell Rep 2013;4:19–30.
29. Chang JT, Ciocca ML, Kinjyo I, Palanivel VR, McClurkin CE, Dejong CS, et al. Asymmetric proteasome segregation as a mechanism for unequal partitioning of the transcription factor T-bet during T lymphocyte division. Immunity 2011;34:492–504.
30. Adikrisna R, Tanaka S, Muramatsu S, Aihara A, Ban D, Ochiai T, et al. Identification of pancreatic cancer stem cells and selective toxicity of chemotherapeutic agents. Gastroenterology 2012;143:234–45 e7.

Social and biological factors influencing the outcomes of children with Wilms tumors in Kenya and other Sub-Saharan countries

Kazuko Kumon[1], Yasuhiko Kaneko[2]

[1]Child Doctor Medical Centre, Kenya PO box 5828-00200, Nairobi, Kenya; [2]Research Institute for Clinical Oncology, Saitama Cancer Center, Ina, Saitama 362-0806, Japan

Corresponding to: Yasuhiko Kaneko, MD. Research Institute for Clinical Oncology, Saitama Cancer Center, Ina, Saitama 362-0806, Japan. Email: kaneko@cancer-c.pref.saitama.jp.

Abstract: Wilms tumor (WT) is a common pediatric solid tumor, and the 5-year event-free survival rate of patients with this tumor has reached 85-90% in developed countries, whereas those in developing countries were reported to be less than 50%. To overcome these disparities, physicians and investigators in developed and developing countries are currently performing research with the aim of the better management of children with WT in Kenya and other Sub-Saharan countries. Axt and colleagues published a study that increased understanding of clinicopathology of WT in Kenya on the basis of a comprehensive web-based WT registry. The study revealed that patients enrolled in the National Health Insurance Fund (NHIF) showed better completion rate of therapy and better event-free survival than those not enrolled, indicating insufficient health coverage for those not enrolled in the NHIF. Approximately 20-30% of Kenyan population is estimated to be covered by some forms of health insurance, mostly by the NHIF. This could be improved through various approaches. The report described that 2-year event-free survival rate was 52.7% for all patients, although loss to follow up was 50%; the findings indicate large problems both in the study results and also in the completion of treatment. It is crucial to determine at which point patients stopped their treatment and why. The development of standardized treatment protocol for WT is an urgent agenda. We hope that researchers in developed countries and health providers in Kenya can work together in future to conquer disparities in the outcomes of children with WT.

Keywords: Wilms tumor (WT); disparities of outcomes; Lost to Follow Up (LTFU); Kenya

Submitted Jan 18, 2014. Accepted for publication Jan 20, 2014.
doi: 10.3978/j.issn.2224-4336.2014.01.08
Scan to your mobile device or view this article at: http://www.thetp.org/article/view/3230/4105

Wilms tumor (WT) is a common pediatric solid tumor, and the event-free survival rate of patients with this tumor is high in developed countries (1). WT as well as Burkitt lymphoma and Kaposi sarcoma are target cancers in Sub-Saharan Africa, in which limited resources are available (2), because the incidence of WT is high among pediatric cancers in Africa, and a high cure rate may be accomplished if standardized therapy could be more accessible. Epidemiological studies showed that the incidence of WT was high in Africa, low in Asia, and intermediate in Caucasian in North America (3). Furthermore, the incidence of WT in Asians was shown to be approximately one half to two-thirds of that in Caucasians in Hawaii and Britain (4,5), and was higher in Black American than in Caucasians in USA (3). These findings suggest that the different incidence rates among the three populations may be caused by different genetic backgrounds, and not environmental factors. The 5-year event-free survival rates of patients with WT in developed countries has reached 85-90%, whereas those in developing countries were reported to be 50% or less (1,6,7). To overcome these disparities, physicians and investigators in developed and developing countries are currently performing research with the aim of the better management of children with WT in Kenya and other Sub-Saharan countries (8).